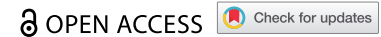


REPORT



## Rapid discovery of diverse neutralizing SARS-CoV-2 antibodies from large-scale synthetic phage libraries

Tom Z. Yuan<sup>a</sup>, Pankaj Garg<sup>b</sup>, Linya Wang<sup>a</sup>, Jordan R. Willis<sup>c</sup>, Eric Kwan<sup>a</sup>, Ana G Lujan Hernandez<sup>a</sup>, Emily Tuscano<sup>a</sup>, Emily N. Sever<sup>a</sup>, Erica Keane<sup>d</sup>, Cinque Soto<sup>e</sup>, Eric M. Mucker<sup>f</sup>, Mallorie E. Fouch<sup>g</sup>, Edgar Davidson<sup>g</sup>, Benjamin J. Doranz<sup>g</sup>, Shweta Kailasan<sup>h</sup>, M. Javad Aman<sup>h</sup>, Haoyang Li<sup>i</sup>, Jay W. Hooper<sup>f</sup>, Erica Ollmann Saphire<sup>ij</sup>, James E. Crowe<sup>ikl</sup>, Qiang Liu<sup>a</sup>, Fumiko Axelrod<sup>a</sup>, and Aaron K. Sato<sup>a</sup>

<sup>a</sup>Twist Biopharma, Twist Bioscience, South San Francisco, CA, USA; <sup>b</sup>Alamar Biosciences, Fremont, CA, USA; <sup>c</sup>IAVI Neutralizing Antibody Center, Scripps Research, La Jolla, CA, USA; <sup>d</sup>Neuroscience Research Institute, Department of Molecular, Cellular, and Developmental Biology, University of California, Santa Barbara, CA, USA; <sup>e</sup>Vanderbilt Vaccine Center, Vanderbilt University Medical Center, Nashville, TN, USA; <sup>f</sup>United States Army Medical Research Institute of Infectious Diseases, Fort Detrick, Frederick, Maryland, USA; <sup>g</sup>Integral Molecular, Philadelphia, PA, USA; <sup>h</sup>Integrated BioTherapeutics, Inc. Rockville, MD, USA; <sup>i</sup>Center for Infectious Disease and Vaccine Research, La Jolla Institute for Immunology, La Jolla, CA, USA; <sup>j</sup>Department of Medicine, University of California San Diego, La Jolla, CA, USA; <sup>k</sup>Department of Pathology, Microbiology, and Immunology, Vanderbilt University Medical Center, Nashville, TN, USA; <sup>l</sup>Department of Pediatrics, Vanderbilt University Medical Center, Nashville, TN, USA

### ABSTRACT

Coronavirus disease 2019 (COVID-19) is an evolving global public health crisis in need of therapeutic options. Passive immunization of monoclonal antibodies (mAbs) represents a promising therapeutic strategy capable of conferring immediate protection from SARS-CoV-2 infection. Herein, we describe the discovery and characterization of neutralizing SARS-CoV-2 IgG and VHH antibodies from four large-scale phage libraries. Each library was constructed synthetically with shuffled complementarity-determining region loops from natural llama and human antibody repertoires. While most candidates targeted the receptor-binding domain of the S1 subunit of SARS-CoV-2 spike protein, we also identified a neutralizing IgG candidate that binds a unique epitope on the N-terminal domain. A select number of antibodies retained binding to SARS-CoV-2 variants Alpha, Beta, Gamma, Kappa and Delta. Overall, our data show that synthetic phage libraries can rapidly yield SARS-CoV-2 S1 antibodies with therapeutically desirable features, including high affinity, unique binding sites, and potent neutralizing activity *in vitro*, and a capacity to limit disease *in vivo*.

### ARTICLE HISTORY

Received 4 July 2021  
Revised 12 October 2021  
Accepted 1 November 2021

### KEYWORDS


SARS-CoV-2; neutralizing antibody; COVID-19; spike glycoprotein; synthetic libraries

## Introduction

Severe acute respiratory syndrome coronavirus two (SARS-CoV-2) causes COVID-19, a respiratory infection that can ultimately lead to severe pneumonia, acute respiratory failure, and death. Following the Wuhan outbreak in December 2019,<sup>1–3</sup> SARS-CoV-2 quickly achieved global, pandemic spread, culminating in 246,889,661 global cases and 5,003,021 global deaths as of November 1, 2021.<sup>4</sup> Safe and effective therapies are therefore needed to combat the transmissibility, pathogenicity, and disease severity of SARS-CoV-2 as new variants of concern emerge. Passive antibody therapy using either convalescent plasma from recovered COVID-19 survivors or monoclonal antibodies (mAbs) has proven safe and effective against other betacoronaviruses such as Middle East respiratory syndrome-related coronavirus (MERS-CoV) and SARS-CoV.<sup>5</sup> Although convalescent plasma is readily available and approved for use in critically ill COVID-19 patients,<sup>6</sup> it must be screened for blood-borne pathogens, requires high titers for therapeutic efficacy, and can pose rare but nevertheless notable risks, including transfusion-related acute lung injury, transfusion-associated dyspnea, circulatory overload, and allergic reactions.<sup>7,8</sup> These risks can be subjugated through the use of recombinant neutralizing mAbs, the therapeutic agent of convalescent plasma.

SARS-CoV-2 hijacks the same host cell entry mechanism as its predecessor SARS-CoV. Similar to SARS-CoV, SARS-CoV-2 uses the trimeric spike (S) to enable cell entry.<sup>9,10</sup> These glycoproteins are made up of two subunits (S1 and S2) and decorate the surface of the virion. The subunits stochastically switch between “up” and “down” states. The former conformation exposes the receptor-binding domain (RBD) of the S1 subunit that interacts with human angiotensin-converting enzyme 2 (ACE2).<sup>11</sup> Upon binding ACE2, S1 becomes locked in the less stable “up” conformation, and a conformational change in the S2 subunit propels the virion toward the host cell’s membrane. Proteolytic processing of S by the host cell transmembrane protease TMPRSS2 enables the subsequent fusion of the virion to the host cell membrane. Neutralizing mAbs isolated from convalescent patient B cells primarily target the RBD on S1 and either block it from interacting with ACE2<sup>12</sup> or trap S in the destabilized “up” position, causing it to unfold prematurely into a post-fusion configuration in the absence of a cellular target, rendering the virus fusion-incompetent.<sup>13</sup> Roughly, half of neutralizing antibodies found in the convalescent plasma of COVID-19 survivors bind S1, and the most potently neutralizing among them target the

**CONTACT** Aaron K. Sato Twist Biopharma, Twist Bioscience, 681 Gateway Blvd,  [asato@twistbioscience.com](mailto:asato@twistbioscience.com)  South San Francisco, CA 94080, USA

 Supplemental data for this article can be accessed on the [publisher's website](#)

© 2021 The Author(s). Published with license by Taylor & Francis Group, LLC.

This is an Open Access article distributed under the terms of the Creative Commons Attribution-NonCommercial License (<http://creativecommons.org/licenses/by-nc/4.0/>), which permits unrestricted non-commercial use, distribution, and reproduction in any medium, provided the original work is properly cited.

RBD while the remaining antibodies target the NTD.<sup>12,14,15</sup> Despite the prevalence of RBD-targeting mAbs, neutralizing mAbs that target S domains outside of RBD continues to be isolated from convalescent COVID-19 patients.<sup>12,16,17</sup> Although S1 RBD represents a prime target for the development of neutralizing mAbs against SARS-CoV-2, identifying neutralizing mAbs with alternative binding sites to more conserved regions of the S protein should be pursued to combat emerging variants of concerns that primarily focus escape mutations at the RBD.<sup>18</sup> Alternate epitope targets to more conserved regions could work synergistically in “cocktail” therapeutics. Such cocktails may help minimize mutagenic escape by simultaneously targeting distinct epitopes on SARS-CoV-2 S1 and, perhaps, by engaging multiple neutralization mechanisms.

Although antiviral mAbs can be isolated directly from recovered survivors, phage display offers many advantages for mAb discovery and development, particularly in the context of the COVID-19 pandemic. During phage display, antibody genes are inserted into phage coat protein genes to enable affinity selection of antibody-expressing phage particles by biopanning. Knowledge of the antibody gene enables rapid tuning of antibody properties, including affinity and specificity, and facilitates their subsequent humanization and multimerization. Phage display can also be used to screen single-domain camelid antibodies (also known as VHH antibodies or nanobodies). The VHH format may provide higher stability and greater access to viral and host protein epitopes due to its small size. These features make nanobodies attractive in the context of the COVID-19 pandemic for a number of reasons: they can be manufactured more easily and cheaply than IgGs,<sup>19</sup> engineered as multimers<sup>19</sup> and nebulized for direct delivery to the lungs,<sup>20,21</sup> the primary site of SARS-CoV-2 disease. However, since the small size of nanobodies leads to their rapid clearance in the kidney even in multimeric forms,<sup>22</sup> fusing an Fc domain is typically necessary to improve half-life.<sup>19</sup>

Here, we designed, synthesized, and screened four large-scale phage libraries for neutralizing antibodies that block SARS-CoV-2 infection (Table 1). In constructing these libraries, we used a synthetic approach to generate complementarity-determining region (CDR) diversity in the hypervariable region, enabling higher precision in sequence diversification than methods based on degenerate oligonucleotides.<sup>24,25</sup> For each of the four libraries, oligo pools encoding each of the CDR loops were synthesized by Twist Bioscience and assembled into single-chain variable fragment (scFv), antigen-binding fragment (Fab), or single-domain VHH formats in human or humanized frameworks. Our synthetic approach leverages solid-phase oligo synthesis using a silicon-based nanowell platform (WO 2015021080) that can synthesize highly diverse libraries *en masse* with very low error rates.<sup>25</sup> We report the discovery and characterization of diverse neutralizing mAbs against SARS-CoV-2 from four synthetic antibody libraries. A subset of antibodies, when alone or in combination, limited disease when administered pre- or post-exposure to SARS-CoV-2 in an animal model.

## Results

### Design, construction, and screening of anti-S1 antibody phage libraries

As part of our antibody discovery pipeline, we generated four phage antibody libraries for screening against the SARS-CoV-2 S1 (GenBank QHD43416.1, residues 16–685). We maximized the CDR diversity of our libraries based on the repertoires from human and/or llama CDR sequences as described below, which we subsequently synthesized and assembled into antibody hypervariable regions for phage display (Figure 1(a)). We created four such libraries: 1) scFv library constructed using CDRs identified in the memory B cells of a convalescent COVID-19 donor (TB181 COVID-19 scFv); 2) an antigen-binding fragment (Fab) library constructed using CDRs from human naïve and memory B cells (TB182 Fab); 3) a humanized llama nanobody library with shuffled, llama-based CDR diversity (TB201 VHH); 4) a humanized llama nanobody library constructed using natural llama CDR1/2 sequences and human CDR3s identified from human naïve and memory B cells (TB202 VHH).

CDR diversity for the TB181 COVID-19 scFv library was provided by the Crowe laboratory at Vanderbilt University Medical Center. Each library possessed a diversity of  $>10^{10}$  (see Materials and Methods for additional details). Antibodies were selected for SARS-CoV-2 S1 binding using a bead-based biopanning strategy. For each library, phages were selected over four rounds of panning (Supplemental Table 1) to identify putative high-affinity S1-binding antibodies. After panning, enzyme-linked immunosorbent assay (ELISA) was used to assess the binding of phage-displayed antibodies to S1 protein. Antibody candidates from each library that elicited a greater than 3-fold enrichment over a bovine serum albumin (BSA) control protein were selected as initial leads. From the TB181 COVID-19 scFv, TB182 Fab, TB201 VHH, and TB202 VHH libraries, we identified 41, 14, 68, or 112 unique clones, respectively.

Following phage display ELISA screening, S1-binding antibody candidates were reformatted to human IgG1 (TB181 COVID-19 scFv, TB182 Fab) or a VHH-Fc fusion containing the Fc region of human IgG1 (TB201 VHH, TB202 VHH) for further characterization and development.

### Biophysical characterization and competition binning of antibody candidates

In total, we identified 235 S1-binding leads across the four phage libraries. We first characterized the binding affinity and specificity of our S1 antibody candidates using surface plasmon resonance (SPR) and S1 RBD-ACE2 competition assays, respectively. We identified multiple S1 antibody candidates with nanomolar affinities against SARS-CoV-2 S1, including TB181-4 ( $K_D = 83$  nM), TB182-4 ( $K_D = 21$  nM), TB182-7 ( $K_D = 25$  nM), TB201-1 ( $K_D = 6.6$  nM), TB202-3 ( $K_D = 32$  nM), and TB202-63 ( $K_D = 46$  nM) (Figure 1(b); see Figure 2 for SPR data from all leads). Additionally, all but one of these candidates are bound to the prefusion-stabilized SARS-CoV-2 S trimer with picomolar affinities (Figure 1(b)). We also assayed the cross-

**Table 1.** All phage-displayed antibody libraries were designed by assembling synthesized oligo pools encoding CDRs as human scFv and Fab or humanized single domain nanobody (VHH) fragments fused to the attachment protein gene 3 protein (G3P). TB181 COVID-19 scFv incorporates germline gene segments encoding heavy chain VH3–23 and light chain VL2–23. The TB182 Fab library uses VH3–23 and VK1–39. Both VHH libraries use a humanized DP-47 framework.<sup>23</sup> The number of phage binders identified from the Round 4 panning output of each library is listed along with the number of unique antibodies discovered. Following phage panning and screening, a total of 235 antibody fragments were converted to either human IgG1 or a VHH-Fc fusion containing the Fc region of human IgG1 for further characterization of the purified antibody.

Library	Phage-displayed Antibody Format	Framework	CDR Diversity Source	Phage Binders Identified (Unique)	Purified Antibody Format
TB181 COVID-19 scFv	scFv	IGHV3–23IGLV2–23	Memory B cells from convalescent COVID-19 donor	478(41)	IgG1
TB182 Fab	Fab	IGHV3–23IGKV1–39	Human naïve and memory B cells	235(14)	IgG1
TB201 VHH	VHH	Humanized DP-47	Llama immune repertoires	342(68)	VHH-Fc
TB202 VHH	VHH	Humanized DP-47	Llama immune repertoires (CDR1, CDR2) and human naïve and memory B cells (CDR3)	403(112)	VHH-Fc

binding of antibody candidates to the S1 domain of SARS-CoV S protein. All antibody candidates specifically bound SARS-CoV-2 S1 except for TB182–3 and TB182–4, which both cross-bound with SARS-CoV spike protein

(Supplemental Figure 1). We further investigated the binding of S1 antibody candidates to ACE2 in an ELISA (Figure 1(c)) and flow cytometric competition binding assays (Figure 1(d); see Figure 2 for flow cytometry data

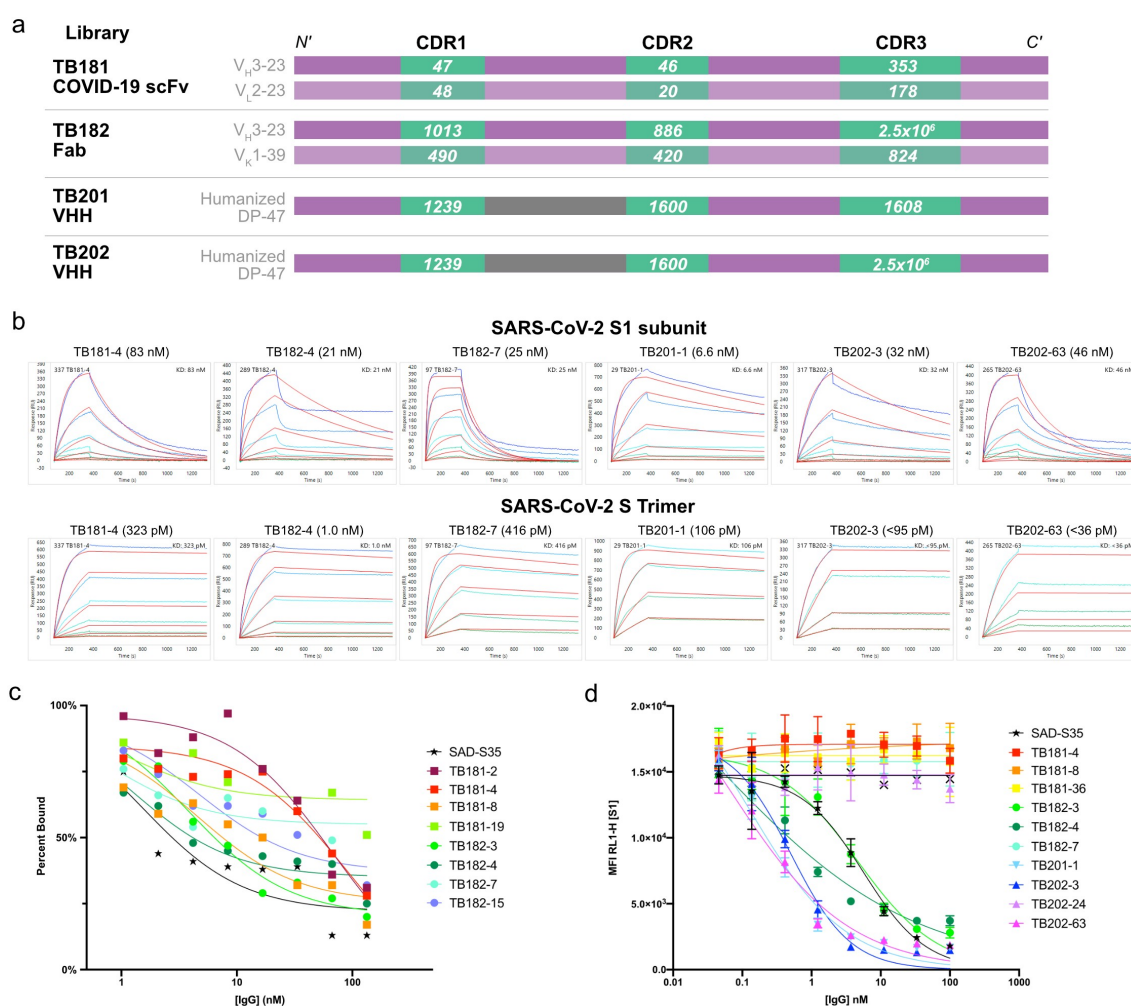


**Figure 1.** Identification of high-affinity mAbs against SARS-CoV-2 S1 subunit and pre-fusion stabilized S trimers. (a) Schematic of antibody library designs used in phage panning. Numbers on white text on green indicate the number of CDRs represented within each oligo pool per library. Purple blocks represent human or humanized germline framework regions; gray blocks represent llama framework regions. (b) Binding affinity of lead antibodies, as determined by SPR, demonstrating nanomolar binding to the SARS-CoV-2 spike S1 subunit. Leads from TB181 COVID-19 scFv and TB182 Fab libraries were reformatted and expressed as IgG1, while leads from TB201 VHH and TB202 VHH libraries were converted to VHH-Fc. Apparent binding affinity to spike trimers stabilized in the pre-fusion conformation are in the picomolar range.<sup>26</sup> SPR experiments were performed on a Carterra LSA SPR biosensor, binding affinities were calculated by fitting to 1:1 model in Carterra Kinetics Tool software. See Materials and Methods for complete assay description. (c) Competition ELISA showing decreasing levels of S1 RBD binding to immobilized ACE2 on Nunc Maxisorp plates with increasing concentrations of antibody. The experiment was performed in singlicate. (d) Inhibition flow cytometry experiment showing lowering levels of S1 RBD binding to Vero E6 cells expressing ACE2 as measured by decreasing mean fluorescence intensity (MFI) as antibody concentrations increase. The experiment was performed in triplicate with standard deviation shown as error bars.



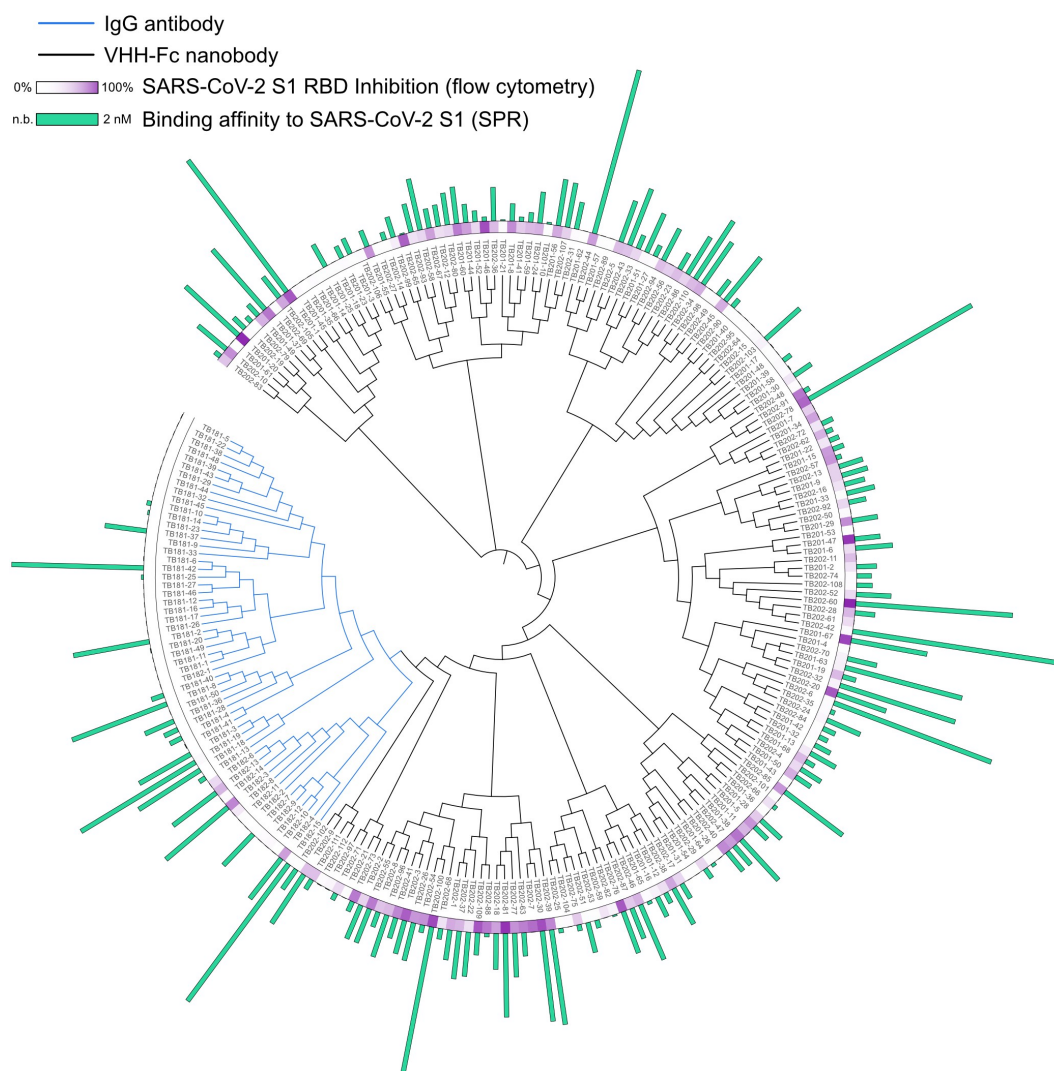


**Figure 2.** Sequence diversity and characterization of 235 SARS-CoV-2 S1-binding antibodies. Phylogenetic tree of SARS-CoV-2 S1-binding IgG (blue lines) and VHH-Fc (black lines) candidates identified by phage display. Green bars represent the binding affinity of each candidate as measured by SPR. Relative binding affinity is displayed linearly, a longer bar indicates improved binding affinity. The longest bar represents an observed binding affinity of 2 nM, the shortest visible bar represents 6.6  $\mu$ M. No bar indicates no binding observed. Purple gradient represents the percent inhibition of each antibody in the Vero E6 competition assay at 100 nM mAb, weak inhibitors are represented in white, strong inhibitors are represented in purple. Phylogenetic tree data generated by aligning variable heavy sequences with Multiple Sequence Comparison by Log-Expectation (MUSCLE).<sup>27</sup> circular dendrogram figure constructed using interactive tree of life (iTOL).<sup>28</sup>

from all leads). For the flow cytometry assay, we incubated each mAb candidate with recombinant SARS-CoV-2 S1 RBD and Vero E6 cells, which are susceptible to SARS-CoV-2<sup>29</sup> and SARS-CoV-2<sup>12</sup> infection via ACE2. Many high-affinity anti-S1 mAbs effectively blocked the interaction between SARS-CoV-2 S1 RBD and ACE2 on Vero E6 cells as measured by flow cytometry, including TB182-3, TB182-4, TB201-1, and TB202-63, to name a few (Figure 1(d)). Nonetheless, some high-affinity, S1-binding candidates such as TB202-42 and TB181-8 failed to block this interaction. Notably, TB181-8 did compete with ACE2 in the less physiologically relevant ELISA assay.

Next, we examined the sequence diversity of each candidate. Given the diverse sources of CDR repertoires that we used to design these libraries, we used phylogenetic clustering analysis to investigate sequence signatures that may be common between antibodies isolated from different libraries. Indeed, antibody candidates from libraries containing common CDR

sources clustered into similar clonal families. For example, many TB201 and TB202 candidates – both of which contained natural llama CDR 1/2s – were found in closely related sequence families.

We next investigated the cross-competition of the S1 antibody candidates and existing SARS-CoV-2 antibodies, including CR3022 and SAD-S35 (Acro Biosystems), with S1 using high-throughput SPR (HT-SPR). This assay revealed four competition bins: namely, two bins that overlapped serially, and two additional, independent bins (Figure 3). The first bin (bin 1) included numerous VHH (TB201) candidates and SAD-S35. CR3022 competed with a few TB182 candidates in bin 2. TB182-4 bridged bins 1 and 2, forming a bin with CR3022 and SAD-S35. The remaining bins, 3 and 4, exhibited no overlap. Bin 3 included TB182-7, TB181-4, TB181-41, and TB181-18. Bin 4 only contained TB202-24, suggesting that it binds a unique epitope not targeted by our other candidates. We note that the bins



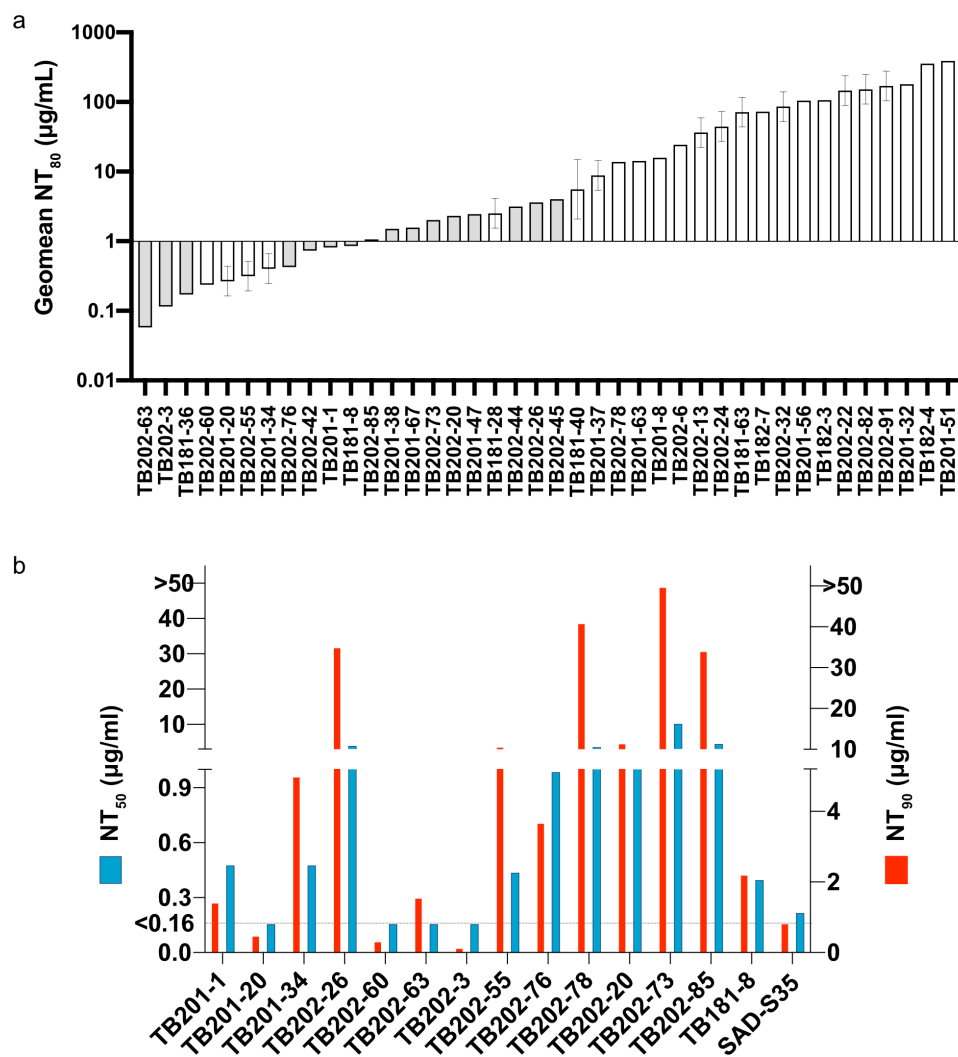


**Figure 4.** Neutralizing activity of top antibody candidates. (a) 40 blinded samples were tested in a PRNT (at USAMRIID) using the authentic SARS-CoV-2 Washington isolate. All samples were run in at least two independent assays. Shaded bars indicate only one value used to determine titer, where the first assay used in a dilution series does not reach an endpoint titer. The NT<sub>80</sub> value was calculated by dividing the sample concentration by PRNT<sub>80</sub> titer. NT<sub>80</sub> values were sorted lowest to highest, or most potent to least potent. (b) in a separate experiment conducted by IBT, IgG and VHH antibodies again demonstrated potent neutralization in an authentic SARS-CoV-2 PRNT. NT<sub>50</sub> and NT<sub>90</sub> represent the antibody concentration required to reduce the number of plaques by 50% or 90%, respectively, compared to free virus.

assay using an immunosuppressed Syrian hamster model<sup>31</sup> performed at USAMRIID and (2) a post-challenge hamster model adapted from Tostanoski *et al.*<sup>32</sup> and performed by IBT. The most potently neutralizing antibodies from each authentic virus PRNT were selected for testing in each model. For the USAMRIID model, TB202-3, TB202-63, and TB181-36 were tested alongside convalescent plasma; for the IBT model, TB202-3 alone was tested. In the pre-challenge model (USAMRIID, Figure 5(a-c)), all three candidates were protective, as indicated by the lack of body weight change compared to hamsters treated with a negative isotype control mAb (c7D11<sup>33</sup>). The VHH antibodies (TB202-3, TB202-63) were as potent as convalescent plasma at 1 mg/kg. The IgG candidate TB181-36 was as effective as convalescent plasma at the 5 mg/kg and 10 mg/kg doses, but not with the 1 mg/kg dose (Supplemental Figure 5). In the post-challenge hamster model, treatment with TB202-3 at 6 hours and 48 hours post-exposure significantly reduced the amount of weight loss at days 5 to 7 post-exposure, which is the time that immediately followed peak disease in this model (Figure 5(d-e)). Early intervention

appeared important to the efficacy of TB202-3 in this post-challenge model, as later dosing schedules were less effective at attenuating the disease course. Additionally, viral load as measured by fifty percent tissue culture infective dose (TCID<sub>50</sub>) was significantly reduced in the lungs relative to vehicle control ( $p < .0001$ , 2-way ANOVA, Figure 5(g)).

We finally evaluated an antibody cocktail consisting of a 1:1 ratio of TB181-36 and TB202-63 in the post-exposure hamster model. To determine whether combining these candidates could halt the progression of SARS-CoV-2 infection in already infected hamsters, we administered the antibody cocktail 1–6 days post-inoculation. Male and female cyclophosphamide-suppressed hamsters treated with a one-time dose of 20 mg/kg antibody cocktail on days 1 or 2 post-inoculation were protected from weight loss (Figure 6(a-b)). Notably, this model demonstrates relatively high viral titers in the lung by day 2 post-inoculation, indicating that this post-exposure treatment was effective in hamsters with high viral loads (Figure 6(c)). Hamsters treated on days 3, 4, 5, or 6 still

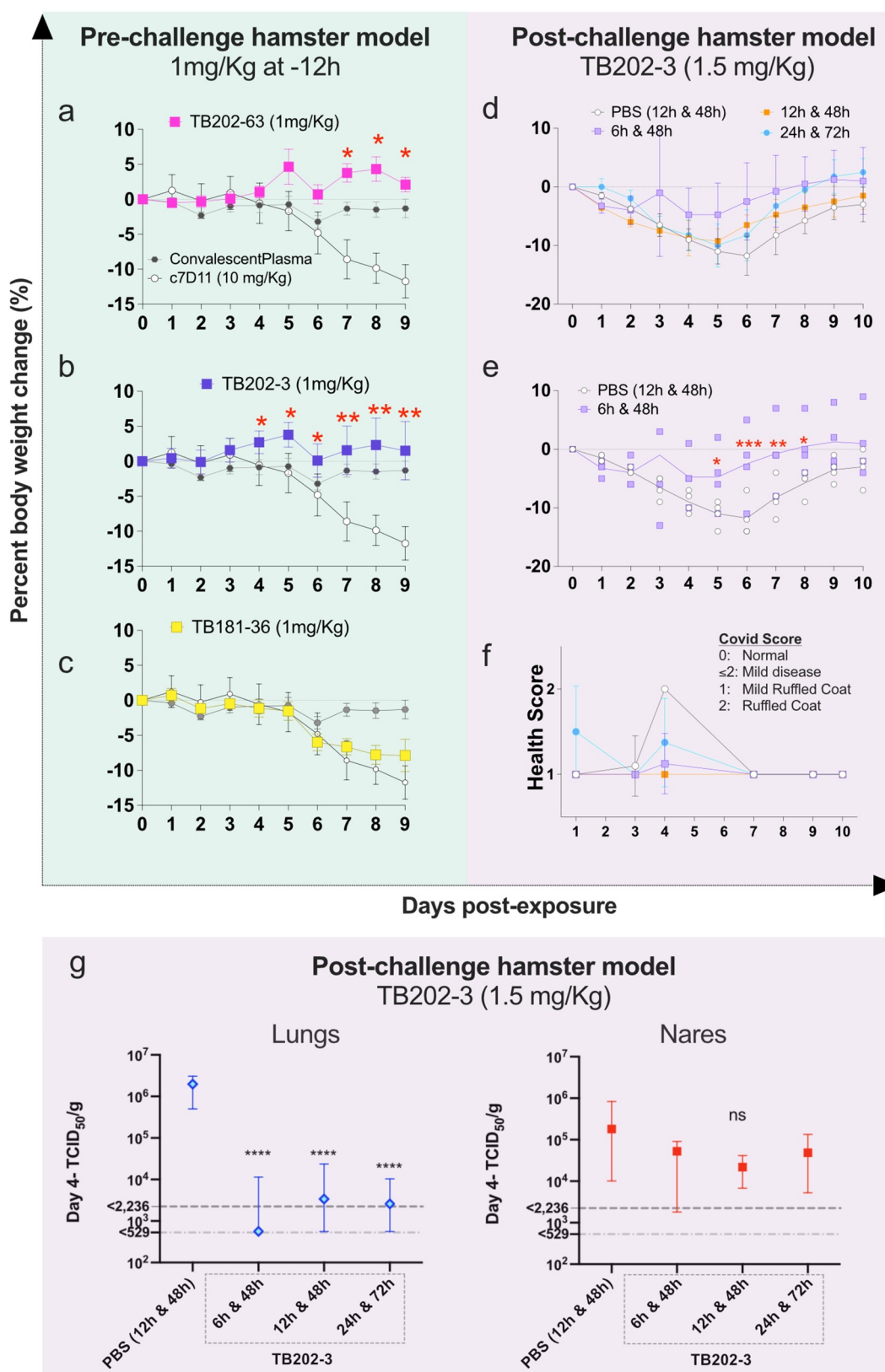


**Figure 5.** Hamster challenge models. (a-c) In a pre-challenge hamster challenge model,<sup>31</sup> administration of monoclonal antibodies 12 hours prior to SARS-CoV-2 (WA1) infection prevented weight loss. TB202-3 and TB202-63, both in VHH-Fc format, conferred protection from weight loss at 1 mg/kg relative to isotype control c7D11 (\* $p < .05$ , \*\* $p < .01$ ). The IgG TB181-36 conferred protection at 5 mg/kg and 10 mg/kg (see supplemental Figure 5). Data is plotted as mean  $\pm$  standard error of mean. (d) post-challenge efficacy study of TB202-3 (1.5 mg/kg) with high-dose intranasal SARS-CoV-2 infection in golden syrian hamsters at various time points between day 0 and day 3 (*i.e.*, 6 and 48 hours, 12 and 48 hours, 24 and 72 hours). (e) TB202-3 conferred significant protection in percent weight change at days 5–8 with the 6- and 48-hour dosing regimen (\* $p < .05$ , \*\* $p < .01$ , \*\*\* $p < .001$ ) (f) health scores from the experiment shown in Figure 5d of hamsters at days 1–14 post-exposure. (g) post-challenge hamsters were sacrificed on day 4 to measure viral load in lung and nares following treatment with TB202-3 at various timepoints. Significant reduction of viral titers was observed in the lungs ( $p < .0001$ , 2-way ANOVA) relative to vehicle only control. Some reduction in titers was observed in the nostrils, however the decrease was not statistically significant. No detectable virus was observed in the spleen or brain. All studies described in this figure were managed by integrated biotherapeutics and performed at a BSL-3 subcontractor facility (BIOQUAL, rockville Md).



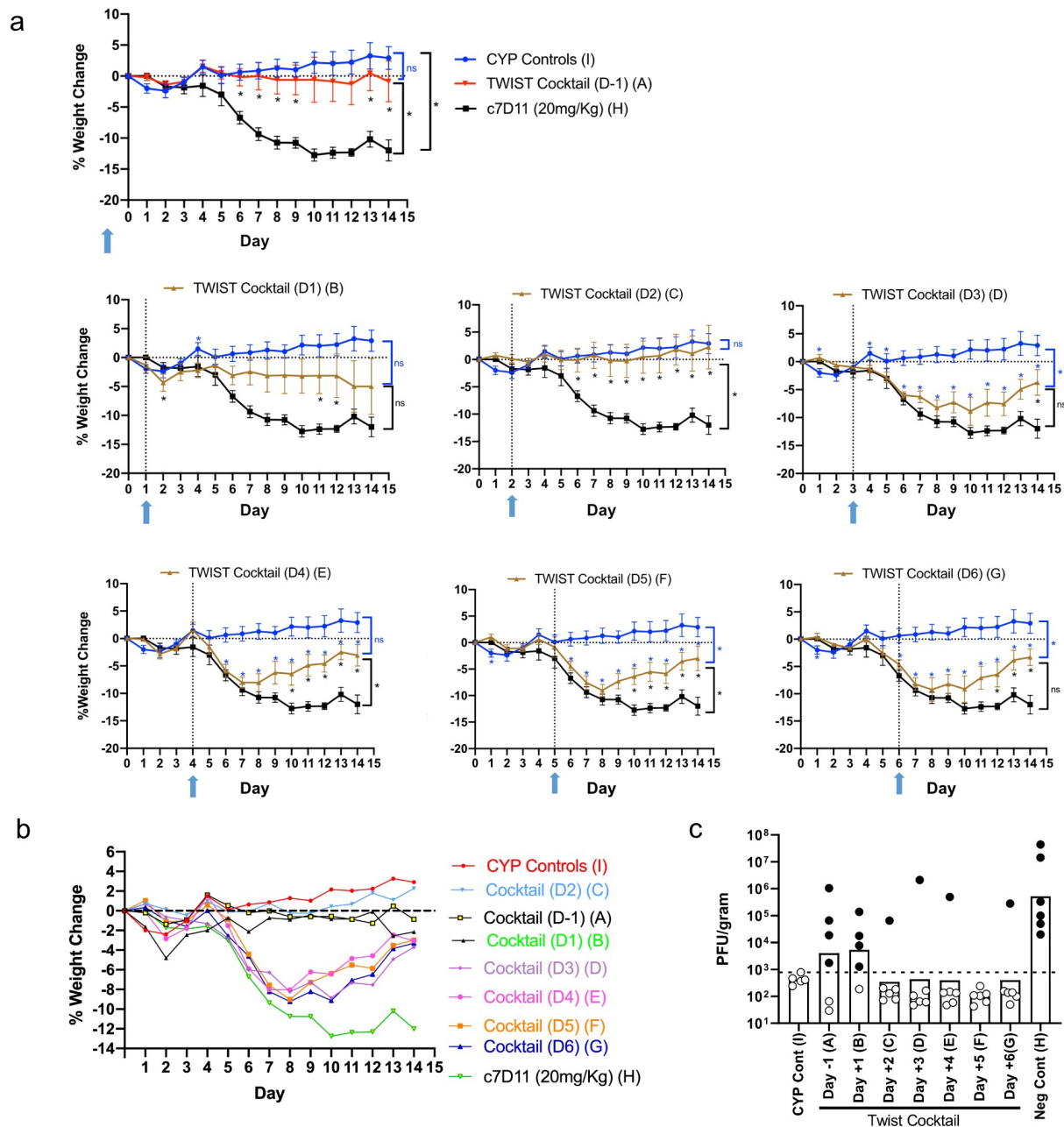


**Figure 6.** Effect of antibody cocktail treatment post-exposure in hamster challenge model (USAMRIID). (a) Animals were immunosuppressed and then exposed to SARS-CoV-2 virus, WA1 strain, on Day 0. Antibody cocktail containing TB181–36 and TB202–63 was administered on the indicated day post-exposure (D1, D2, etc marked by blue arrow, corresponding to Groups B–G). A control group received the cocktail on Day –1 (D-1, Group A). A group was immunosuppressed but not exposed to virus (cyclophosphamide [CYP] control, group i). An IgG monoclonal (c7D11<sup>33</sup>) was administered to Group H as a negative control. Data is presented as mean  $\pm$  standard error of mean, \* $p < .05$ , \*\* $p < .01$ . Experimental groups and all common events are listed in Supplemental Table 3. (b) Percent weight change from all groups, same data from Fig 6a plotted in one graph. (c) Infectious virus in lungs of hamsters on day 14. Lung homogenates were assayed for infectious virus by plaque assay, plaque forming units (PFU) per gram of tissue were calculated and plotted. The limit of the assay is shown as a dotted line. Bars are the geometric means for each group. Groups are denoted in parentheses. White symbols indicated no infectious virus was detected.

experienced weight loss in the days following infection; however, most began to regain weight after day 9 post-infection (Figure 6(a-b)).

### Epitope mapping of top antibody candidates

Having identified several neutralizing mAbs, we sought to clarify their binding epitopes. Based on the aggregate data from the Vero E6 flow cytometry assay, competition binning analysis, and neutralization assays, we hypothesized

that many of our candidates bound divergent sites on SARS-CoV-2 S1. To test this, we generated a shotgun mutagenesis library of SARS-CoV-2 S protein RBD mutants and screened the binding of neutralizing candidates to cells expressing these mutants. This approach allowed us to define which amino acids were critical to the binding of each neutralizing antibody. As shown in Figure 7, most neutralizing mAbs bound the RBD, although the overall binding pattern of the VHH RBD-binding mAbs (TB202–1, TB202–3, and TB202–63) differed from that of the IgG



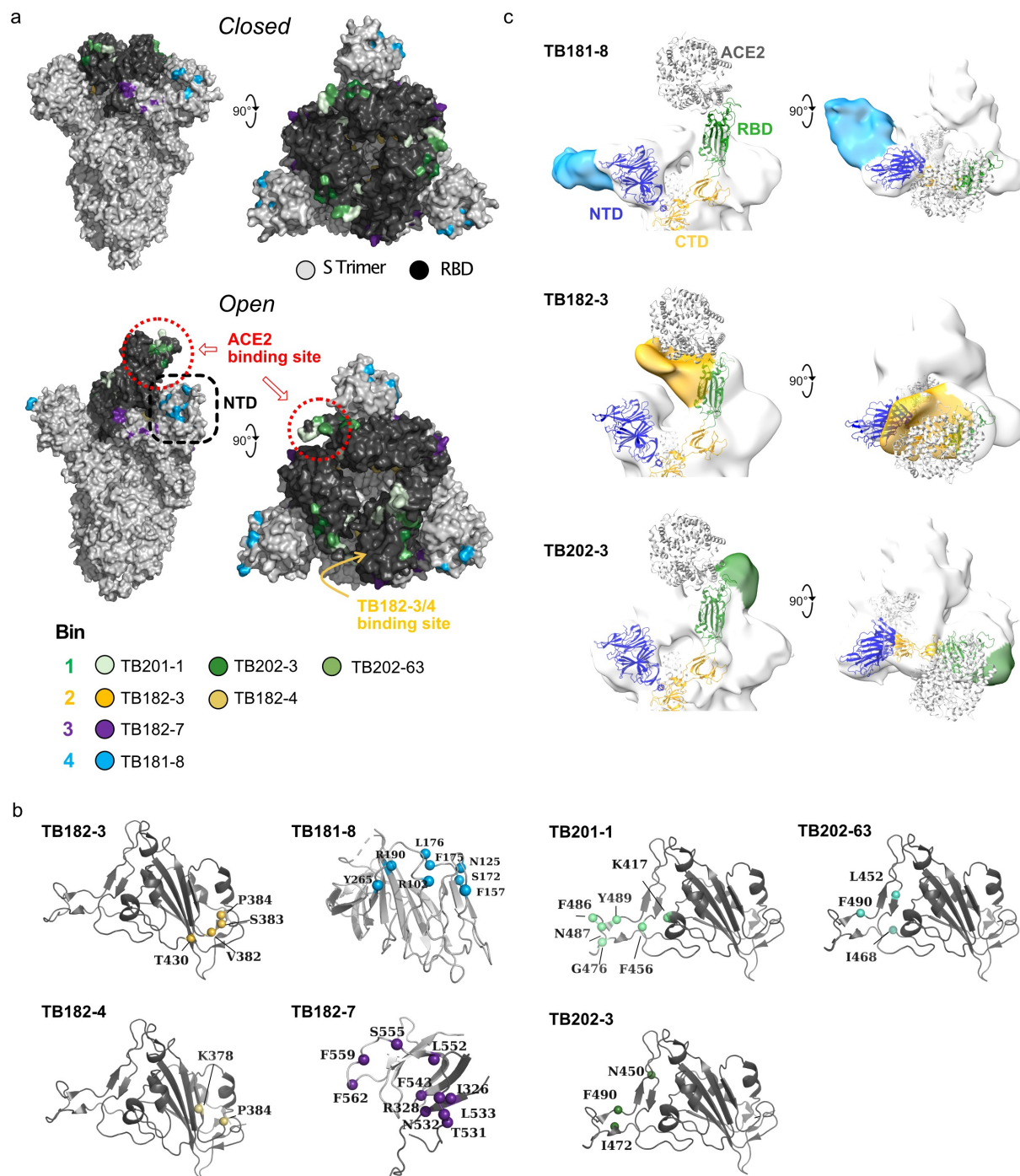


**Figure 7.** Epitope mapping of SARS-CoV-2 S1-binding antibodies. (a) Solvent-accessible surface representation of spike protein trimer in closed (PDB: 6VXX) and open (PDB: 6VSB) conformations. VHH-Fc nanobodies (TB201, TB202) binding sites overlap with that of ACE2 in both conformations, while TB181 and TB182 IgGs access a more occluded region. (b) Cartoon representation of SARS-CoV-2 S protein RBD with critical residues highlighted as spheres for each monoclonal antibody. (c) Negative-staining electron microscopy analysis shows the distinct binding regions of antibodies identified from the distinct antibody libraries used in this study (colored surface). The SARS-CoV-2 spike protein NTD, C-terminal domain (CTD), RBD and bound ACE2 are shown as cartoon representations.

RBD-binding mAbs (TB182-3, TB182-4, TB182-7). Whereas residues in the ACE2-binding site of the RBD were critical for the VHH RBD-binders, more occluded residues mediated the binding of the TB182-3 and TB182-4 IgG candidates. TB182-7, an IgG, bound a unique site that extended beyond the RBD (Figure 7(a-c)). Although most of the neutralizing mAbs we mapped bound to S1 RBD, there was one notable exception: TB181-

8. The inability of this candidate to inhibit the binding of S1 RBD to ACE2 in the Vero E6 flow cytometry assay indicated the position of a binding epitope outside the RBD. To clarify this, we extended our shotgun mutagenesis approach beyond the RBD. Critical residues for the binding of TB181-8 were found in the NTD of the S1 subunit (Figure 7).

## Discussion

mAbs represent an attractive therapeutic strategy for COVID-19 due to their long half-life (~3 weeks for IgG) and immediate neutralizing properties.<sup>34</sup> In this study, we used phage display to identify multiple synthetic mAbs that neutralize SARS-CoV-2 infection *in vitro* and *in vivo*. To generate comprehensive phage libraries for screening, we sourced CDR diversity from B cells obtained from naïve and COVID-19-infected individuals, as well as llama immune repertoires. We isolated novel potentially neutralizing mAbs with distinct binding sites as revealed by competition, pseudovirion and live-virus neutralization, and epitope mapping assays. Multiple mAbs (TB202-3, TB202-63, and TB181-36) identified from this process possessed antiviral activity in *in vivo* hamster models of SARS-CoV-2 infection, highlighting their potential for use as COVID-19 therapeutics. Although many neutralizing mAbs against SARS-CoV-2 S1 have been identified already from COVID-19 survivors,<sup>12,15,17,35,36</sup> immunized animals,<sup>19</sup> or by phage display,<sup>37,38</sup> our data support the use of synthetic antibody phage libraries as a means of accessing unique and less immunodominant epitopes.

In parallel to this work, a subset of the antibodies described here were submitted to the Coronavirus Immunotherapeutic Consortium (CoVIC; <https://covic.lji.org/>) to further assess their therapeutic potential.<sup>39</sup> In a blind comparison, each submitted antibody was evaluated side-by-side with other mAbs in 12 standardized assays designed to map their binding epitopes, neutralization profiles, and potential resistance to escape mutations. Assignment of submitted antibodies to distinct epitope “communities” across the RBD and NTD domains of S1 using high-throughput and negative stain electron microscopy (ns-EM) largely confirmed the epitope mapping data shown here while providing additional context on binding mechanisms (see Supplemental Table 2 to see the unblinded CoVIC assignments for Twist submitted mAbs and equivalent epitope communities). Two antibodies from the TB182 Fab library, TB182-3 and TB182-4, clustered in the RBD-7 community (analogous to Bin 2 in Figure 3), a target site situated on the occluded, inner face of the RBD that is accessible only in the “up” position (or “open” conformation) of the Spike protein. TB202-3 and TB202-63, both from the TB202 VHH library, overlapped on the RBD-4 epitope (analogous to Bin 1 in Figure 3), a site that directly mediates the S1-ACE2 interaction in both configurations of the S1 protein (“up” and “down”). TB182-7, an RBD-binder that does not block the S1 RBD-ACE2 interaction, binned with the RBD-5 epitope community situated on the outward edge of RBD. Finally, TB181-8 from the COVID-19 scFv library was confirmed to bind to the NTD in the CoVIC assays, providing another possible avenue for antibody neutralization aside from directly blocking the RBD-ACE2 interaction. Negative-staining electron microscopy (ns-EM) analysis suggests that TB181-8 recognizes a unique region that avoids all the known NTD mutations and binds to a rarely exposed region of the NTD.<sup>39</sup>

The SARS-CoV-2 S protein, which mediates viral entry via the host receptor ACE2, is a key target for neutralizing antibodies.<sup>12,14,15</sup> A cryo-EM of intact SARS-CoV-2 virions demonstrated that the S trimer sparsely populates the virion

surface and exhibits substantial flexibility, providing antibodies with abundant access to virtually the entire Strimer.<sup>40</sup> Yet, most neutralizing anti-S1 antibodies identified in the convalescent plasma of COVID-19 survivors target S1 RBD and neutralize SARS-CoV-2 by directly blocking the S1-ACE2 interaction.<sup>12,14,15</sup> SAD-S35 from Acro Biosystems is one such example.<sup>36</sup> We identified numerous neutralizing VHH antibodies that competed with SAD-S35 in HT-SPR using SARS-CoV-2 S1 (Bin 1, Figure 3), some of which were among the most potently neutralizing antibody clones against authentic SARS-CoV-2 *in vitro* (e.g., TB201-1 and TB202-3; Figure 4). TB202-3 also was protective in pre- and post-challenge hamster infection models (Figures 5,6). The shotgun mutagenesis approach to epitope mapping revealed an overlap between the binding epitopes of representative, SAD-S35-like candidates (namely, TB201-1 and TB202-3) with the ACE2-binding site of S1 RBD (Figure 7). Thus, these VHH candidates likely neutralize SARS-CoV-2 via a similar SAD-S35-like mechanism. SAD-S35 also binds multiple mutational variants of SARS-CoV-2 S1 RBD,<sup>36</sup> a feature that bodes well for the development of SAD-S35-like mAbs.

Antibodies against S1 also neutralize SARS-CoV-2 via an indirect allosteric mechanism. CR3022 binds a cryptic super-site on the inner face of the RBD, situated away from the receptor-binding site and only accessible when S1 is in the open or “up” configuration.<sup>13,39,41–43</sup> Our competition binning assay supports the hypothesis that CR3022 and SAD-S35 antibodies bind distinct, but perhaps closely situated, epitopes<sup>36</sup> because these two reference antibodies binned separately whereas TB182-4 bridged the two bins (Figure 3). Closely related to TB182-4, TB182-3 binned with CR3022, but not SAD-S35. Both TB182-3 and TB182-4 bound occluded sites in the RBD as described above, with P384 (TB182-3, TB182-4) and V382 (TB182-3) serving as key residues for RBD binding (Figure 7). Both residues also participate in the cryptic binding site for CR3022.<sup>41</sup> In addition, TB182-3 and TB182-4 were the only mAbs identified that cross-reacted with SARS-CoV spike S1 subunit (Supplementary Figure 1), which is another feature they share with CR3022. We found that TB182-3 and TB182-4 were both weakly neutralizing in PRNTs using authentic SARS-CoV-2 (Figure 4), similar to reports of CR3022’s weaker neutralizing capabilities.<sup>13,41</sup> CoVIC data independently corroborate the unique binding site, relative lack of ACE2 competition, and weakly neutralizing activity of TB182-3 reported here.<sup>39</sup> Despite their comparatively low neutralizing effects, Lim *et al.*<sup>44</sup> demonstrated that ordinarily non-neutralizing anti-S1 RBD mAbs can enhance the activity of neutralizing anti-S1 RBD mAbs when combined. However, more work is needed to confirm the neutralizing capabilities (or lack thereof) of these antibodies in light of the debate surrounding CR3022’s neutralizing effects<sup>13,41,42</sup> and the discovery of neutralizing mAbs that target the same cryptic RBD supersite.<sup>43,45,46</sup>

One candidate from the COVID-19 scFv library (TB181-8) strongly neutralized SARS-CoV-2 without blocking the binding of SARS-CoV-2 S1 RBD to ACE2 in Vero E6 cells. Shotgun mutagenesis revealed a binding epitope in the NTD of S1 (Figure 7). To date, most discovered SARS-CoV-2 antibodies target the RBD, perhaps due to the frequent use of S1 RBD for

antibody selection.<sup>12</sup> TB181-8 joins a minority of antibodies mapped to the NTD of SARS-CoV-2. The other known NTD-binding antibodies include 4A8,<sup>16</sup> COVA1-22,<sup>17</sup> and several dozen others<sup>12,15,18,47–49</sup> – all mAbs isolated from convalescent COVID-19 patients. Most known NTD antibodies target one of two sites: the NTD supersite on the distal edge from the center of the S trimer (e.g., 4A8) or the flanking “antigenic site V” described by McCallum *et al.*<sup>12,18,49</sup> The most potently neutralizing among these antibodies generally target the NTD supersite.<sup>18</sup> Interestingly, CoVIC data indicate that TB181-8 binds a unique site on the other flanking side of NTD (Figure 7) – an epitope not shared by other known NTD antibodies.<sup>39</sup> Given its unique binding site, how does TB181-8 neutralize SARS-CoV-2, given that anti-NTD antibodies do not compete with ACE2, nor do they prematurely trigger conformational changes in the S protein (the proposed mechanism for CR3022 and similar antibodies)? Instead, they appear to block S-mediated viral fusion at the post-attachment step, although the specific mechanism has yet to be resolved.<sup>18,49,50</sup> Because this mechanism has been proposed for antibodies that bind divergent sites on NTD (*i.e.*, the supersite and antigenic site V), it is plausible that TB181-8 also uses this mechanism. Moreover, the identification of TB181-8 as a unique NTD-binding antibody presents several possibilities for the development of combination antibody therapies. Given their distinct binding sites, neutralization mechanisms, and differential resistance to emerging SARS-CoV-2 strains, NTD antibodies are prime candidates for combination antibody therapy. Indeed, TB181-8 enhanced the neutralizing activity of the RBD-binding TB202-3 in SARS-CoV-2 D614G pseudovirus neutralization assays (Supplemental Figure 2). Alternatively, RBD-binding mAbs that do not compete with ACE2 can be combined with RBD-binders that do, as demonstrated by the improved neutralization we observed when combining TB202-3 and TB182-7 (Supplemental Figure 4).

Several viral variants that escape neutralization by representative mAbs have emerged since the discovery of the original Wuhan SARS-CoV-2 isolate, prompting questions about whether neutralizing mAbs will retain their therapeutic efficacy against the virus as immunodominant epitopes mutate. Indeed, a large portion of neutralizing antibodies that target the RBD or NTD from both convalescent and mRNA vaccine-induced sera are less neutralizing against SARS-CoV-2 strains that contain the E484K spike mutation, including the B.1.351 (Beta) and B.1.1.7 (Alpha) variants.<sup>51,52</sup> Discovery platforms that use synthetic antibodies instead of patient-derived ones can identify antibodies that target key epitopes outside of those altered by mutagenic escape. TB202-3 and TB202-63 are two such antibodies. TB202-3 and TB202-63 neutralize SARS-CoV-2 B.1.351 (Beta) in a pseudovirus assay performed by IBT (Supplemental Figure 3). According to CoVIC data, these antibodies (assigned to the RBD-4 site in Hastie *et al.*<sup>39</sup>) neutralize SARS-CoV-2 by blocking the S1-ACE2 interaction despite binding an epitope outside the core receptor-binding motif of S1. Using SPR, we confirmed that TB202-3 and TB202-63 still bind several mutant S1 and RBD protein targets, including those containing the E484K and N501Y mutations found in

common SARS-CoV-2 variants (Supplemental Figure 6). Both TB202-3 and TB202-63 retain binding to SARS-CoV-2 spike trimer and B.1.351 (Beta), P.1 (Gamma), B.1.617.1 (Kappa) and B.1.617.2 (Delta) spike trimer variants (Supplemental Figure 7). Pseudovirus experiments performed by CoVIC showed that TB202-3 can bind and neutralize B.1.17 (Alpha), B.1.351 (Beta), and P.1 (Gamma) variants. While pseudovirus neutralization by TB202-3 and other mAbs that bind to the RBD-4 epitope are not affected by the single T478K mutation, these mAbs do not neutralize the recently emerged B.1.429 (Epsilon) and B.1.617.2 (Delta) variants that contain the L452R mutation.<sup>39</sup> Further pseudovirus neutralization experiments performed by CoVIC demonstrated that antibodies that bind to epitope communities RBD-5 and RBD-7 (analogous to Bin 3 and Bin 2, respectively) have lower inhibition potency, but are resistant to mutagenic escape from Alpha, Beta, Gamma, Epsilon and Delta variants.<sup>39</sup> TB182-7 binds to RBD-5 and TB182-3 and TB182-4 bind to RBD-7, all three of these mAbs follow this pattern of lower potency relative to the RBD-4 antibodies TB202-3 and TB202-63 (Figure 4(a), Supplemental Table 2).<sup>39</sup> These findings argue that synthetic antibody libraries can be used to access unique epitopes that remain neutralizing in the face of mutagenic escape. TB202-3 and TB202-63 retain their neutralizing activity against some escape mutants, and combining either one with candidates like TB181-8, TB182-7, or TB18-36 (see Figure 6 and Supplemental Figure 4) may further help to minimize mutagenic escape.

Interestingly, there were significant differences in the mAbs identified from each library. MAb from the two VHH libraries generated the most potent neutralizers to WA1 strain (Figures 2, Figures 4), but all nanobody leads fell into a single epitope bin (Bin 1, CoVIC RBD-4). The TB181 COVID-19 scFv library produced one neutralizing antibody that targets a novel NTD epitope (CoVIC NTD-3), but most mAbs from this library did not exhibit strong neutralization (Figure 2). TB182 Fab produced antibodies to CoVIC epitope bins RBD-5 and RBD-7, which tended to have lower neutralization potency but retained activity to single-point mutations and variants of concern in pseudovirus assays.<sup>39</sup>

In conclusion, the antibody discovery workflow described here represents a viable pathway for the rapid identification of antiviral mAbs able to target diverse epitopes. Derived from semi- and fully synthetic libraries, these mAbs bolster the growing list of promising antibody candidates identified by phage display that have previously been reported.<sup>37,53–55</sup> The lead mAbs described here target epitopes outside of the ACE2-RBD binding site that are less prone to mutagenic escape<sup>39</sup> and could be developed as part of a cocktail therapeutic to target distinct sites on the SARS-CoV-2 S protein as has been described for SARS-CoV<sup>23</sup> to both enhance neutralization and retain potency against emerging variants. Investigators are using this strategy in a cocktail comprising four mAbs targeting non-overlapping spike protein epitopes (PolyTope TATX-03).<sup>26</sup> Alternatively, the synthetic mAbs described here



could be used to generate multivalent bispecific constructs capable of targeting multiple sites on SARS-CoV-2 S1, as demonstrated recently by Lim *et al.*<sup>44</sup>

## Materials and methods

### Phage library generation

CDR diversities for all libraries described were screened to remove manufacturing liabilities (such as sequences linked to post-translational modifications), cryptic splice sites, and commonly used nucleotide restriction sites and subsequently encoded by oligo pools synthesized by Twist Bioscience. The COVID-19 scFv phage display library used germline heavy-chain *IGHV3-23* and germline light-chain *IGLV2-23* frameworks and was assembled as scFv by joining the heavy chain variable region (VH) and light chain variable region (VL) with a (Gly4Ser)<sub>3</sub> linker. CDR diversities for COVID-19 scFv phage library were collected with the assistance of collaborators at Vanderbilt University Medical Center from convalescent donors. Both the TB201 VHH and TB202 VHH libraries used a partially humanized DP-47 framework<sup>56</sup> and retained a llama FW2 region to maintain stable expression as a heavy-chain only antibody. The scFv or VHH cassette was then cloned into the pADL-22 c phagemid display vector (Antibody Design Labs) using *Sfi*I restriction digestion before electroporation into TG1 *E. coli* cells (Lucigen). The TB182 Fab library incorporated germline heavy-chain *IGHV3-23* and germline light-chain *IGKV1-39* in a Fab and cloned into a modified, bicistronic pADL-22 c phagemid vector expressing the light chain and heavy chain fused to the attachment protein gene 3 protein (G3P). Each purified phage library had an estimated  $1.0 \times 10^{10}$  diversity as determined by dilution series of colony forming units per milliliter in 2YT agar plates containing 100 µg/ml carbenicillin.

### Panning and screening strategy

Phage particles were blocked with phosphate-buffered saline (PBS) with 5% BSA and depleted for nonspecific binders on M-280 streptavidin coated magnetic beads (Thermo Fisher Scientific). Biotinylated SARS-CoV-2 S1 protein (Acro S1N-C82E8) was mixed with M-280 beads (100 nM per 1 mg bead), washed with PBS/0.5% Tween to remove unbound protein and used as panning target for four rounds of panning. Phage supernatant depleted of nonspecific binders were transferred to bead mixture containing bound biotinylated SARS-CoV-2 S1 and allowed to bind for 1 hour at RT to select for binders with gentle nutation. Following incubation, beads were washed several times with PBS/0.5% Tween to remove non-binding clones. Remaining bound phage were eluted trypsin in PBS buffer for 30 minutes at 37°C. The output supernatant enriched in binding clones was amplified in TG1 *E. coli* cells to use as input phage for the next round of selection, with each round increasing the wash cycles and lowering the total amount of antigen present.

Bacterial colonies containing the phagemid display vector were isolated on 2YT agar plates with 100 µg/ml carbenicillin and single colonies were picked using QPix 420 (Molecular

Devices) into 384-well plates containing 2YT with M13KO7 helper phage (Antibody Design Labs) to express phage for use in ELISAs. Phage ELISAs were conducted using Nunc 384-well plates (Thermo) with passively absorbed SARS-CoV-2 S1 or human ACE2. Anti-M13 antibody conjugated to horseradish peroxidase (HRP) (Sino Biological 11973-MM05T-H) was used to detect the presence of bound phage following the addition of 3,3',5,5'-tetramethylbenzidine substrate. Clones that demonstrated three-fold binding over BSA background were submitted for rolling circle amplification (RCA) and Sanger sequencing to GENEWIZ using phiS4 (GCGGATAACAATTTGAATTCAAGGAGACAG) or psiR2 (CGTTAGTAAATGAATTTTCTGTATGAGG) primers to identify the VH or VL regions, respectively, in TB181 COVID-19 scFv library. VHH libraries were sequenced with phiS4, while the TB182 Fab library used FabseqF1 (GACAGCTATCGCGATTGCAGTGGCAC) or FabseqF2 (TAATTATCAAGGAGACAGTCATAATG) primers for VL or VH regions, respectively.

### Reformatting, expression, and purification of monoclonal antibodies

Variable heavy chain and light-chain domains of anti-SARS-CoV-2 S1 antibodies were reformatted to IgG1, while VHH single-domain antibodies were reformatted to VHH-Fc for DNA back-translation, synthesis, and cloning into mammalian expression vector pTwist CMV BG WPRE Neo utilizing the Twist Bioscience eCommerce portal. Light chain variable domains were reformatted into kappa and lambda frameworks accordingly. Clonal genes were delivered as purified plasmid DNA ready for transient transfection in HEK Expi293 cells (Thermo Fisher Scientific). Cultures in a volume of 1.2 mL were grown to 4 days, harvested and purified using Protein A resin (PhyNexus) on the Hamilton Microlab STAR platform into 43 mM citrate 148 mM HEPES, pH 6. CE-SDS was used to determine antibody purity and confirm molecular weight. A subset of antibodies selected for pseudovirus, live virus and *in vivo* assays was expressed in 30 mL cultures using the same expression system. Cultures were grown for 4 days, harvested, and purified with Phynexus Protein A resin tips on the Hamilton Microlab STAR automated liquid-handling systems. Purified antibodies were concentrated using Amicon, 30 kDa cutoff spin filters. All antibodies were eluted with 50 mM sodium acetate, followed by 140 mM HEPES neutralization buffer to pH 6. Antibodies for *in vivo* studies were further characterized by high-performance liquid chromatography and tested for endotoxin levels (Endosafe® nexgen-PTS™ Endotoxin Testing, Charles River), with less than 5 EU per kg dosing.

### Competition ELISA and flow cytometry assays

The competition ELISA screen used the Acro SARS-CoV-2 inhibitor screening kit (Acro EP-105) and followed the recommended instructions. A 96-well Nunc Maxisorp plate was coated with SARS-CoV-2 S RBD at 0.5 µg/mL for overnight incubation at 4°C. The plate was washed 3× in PBST and blocked with 2% w/v BSA for 1 hr. Following another 3×



wash, biotinylated ACE2 protein was aliquoted to each well at 0.12 µg/mL. Each antibody was then aliquoted to the same plate at decreasing concentrations from 100 nM. The plate is incubated at room temperature (RT) for 1 hr, then washed 3× in PBST. Streptavidin-HRP is aliquoted to at 0.1 µg/mL and incubated once more at RT for 1 hr. The plate is washed 3× in PBST and TMB substrate is aliquoted to each well for 20 min incubation. Sulfuric acid stop solution (1 M) is added to stop the reaction, and the plate is read at 450 nm. SAD-S35, also known as clone HTS0483, was sourced from Acro Biosystems as a positive control (Acro SAD-S35).

Antibodies were also tested in flow cytometry assays to measure inhibition of S1 binding to Vero E6 cells, which constitutively express ACE2. Vero E6 cells were aliquoted in 96-well plates at  $1.5 \times 10^5$  cells per well. Antibodies were diluted in PBS and serially diluted 1:3 from 100 nM. Antibody dilutions are then mixed with 0.1 µg/mL S1 RBD-mFc (Acro SPD-C5259) equally, and incubated at 4°C for 1 hr. The antibody and S1 RBD-mFc mixture then were added to Vero E6 cells, incubated at 4°C for 1 hr, and washed 3× in PBS. APC-conjugated anti-mouse antibody was then aliquoted and incubated for 1 hr at 4°C. Cells were analyzed by flow by measuring the APC signal.

### **SPR affinity measurements and epitope binning of anti-SARS-CoV-2 S1 antibodies**

SPR experiments were performed on a Carterra LSA SPR biosensor equipped with a HC30M chip at 25°C in HBS-TE. Antibodies were diluted to 10 µg/mL and amine-coupled to the sensor chip by EDC/NHS activation, followed by ethanolamine HCl quenching. Increasing concentrations of analyte were flowed over the sensor chip in HBS-TE with 0.5 mg/mL BSA with 5-min association and 15-min dissociation. Commercially sourced SARS-CoV-2 protein reagents were as follows: S1 WA1 (Acro S1N-C52H4), S1 D614G (Acro S1N-C5256), S1 HV69–70del N501Y D614G (Sino Biological 40591-V08H7), S1 HV69–70del Y453F D614G (Sino Biological 40591-V08H8), S RBD WA1 (Acro SPD-C52H3), S RBD N501Y (Acro SPD-C52Hn), S RBD Y453F (Sino Biological SPD-C52Hn), S RBD N439K (Sino Biological 40592-V08H1), S RBD K417N (Sino Biological 40592-V08H5), S RBD E484K (Sino Biological 40592-V08H8), SARS S1 (Acro S1N-S52H5), S Trimer WA1 (Acro SPN-C52H9), S Trimer B.1.1.7 Alpha (Acro SPN-C52H6), S Trimer B.1.351 Beta (Acro SPN-C52Hk), S Trimer P.1 Gamma (Acro SPN-C52Hg), S Trimer B.1.617.1 Kappa (Acro SPN-C52Hr), S Trimer B.1.617.2 Delta (Acro SPN-C52He). Following each injection cycle, the surface was regenerated with  $2 \times 30$ -second injections of IgG elution buffer (Thermo). Data were analyzed in Carterra's Kinetics Tool software with 1:1 binding model.

Epitope binning was conducted in a pre-mix format using similar conditions as above. First, antibodies were amine-coupled to the HC30M chip. Binding test and regeneration scouting showed reproducible binding to SARS-CoV-2 S1 at 50 nM using IgG elution buffer (Thermo). Premixes were then assembled with 250 nM antibody and 50 nM SARS-CoV-2 S1. Data were analyzed in Carterra's Epitope Tool software. Competition assignments were determined relative to the

binding responses for SARS-CoV-2 S1 alone (normalized to 1); premixes giving binding responses less than 0.5 were determined to be competitive, 0.5 to 0.7 were partially competitive, while binding responses above 0.7 were noncompetitive. Heat maps representing the competition results were generated where red, yellow, and green cells represent competitive, partially competitive, and noncompetitive analyte/ligand pairs, respectively. White cells represent unaddressed pairs in the assay.

The binding assays with S trimer complex used HexaPro spike carrying either D or G at amino acid position 614. The HexaPro expression construct we used is modeled after that described by Hsieh *et al.*<sup>57</sup> and involves the introduction of 6 Pro residues that maintain the Spike in a pre-fusion, trimeric conformation, which we have confirmed by negative stain electron microscopy.

### **Epitope mapping**

Epitope mapping was performed essentially as described previously,<sup>58</sup> using a SARS-CoV-2 (strain Wuhan-Hu-1) S protein RBD shotgun mutagenesis mutation library, made using a full-length expression construct for S protein, where residues of S1 were individually mutated to alanine, and alanine residues to serine. Mutations were confirmed by DNA sequencing, and clones arrayed in a 384-well plate, one mutant per well. Binding of mAbs to each mutant clone in the alanine scanning library was determined, in duplicate, by high-throughput flow cytometry. Each S protein mutant was transfected into HEK-293 T cells and allowed to express for 22 hrs. Cells were fixed in 4% (v/v) paraformaldehyde (Electron Microscopy Sciences), and permeabilized with 0.1% (w/v) saponin (Sigma-Aldrich) in PBS plus calcium and magnesium (PBS++) before incubation with mAbs diluted in PBS++, 10% normal goat serum (Sigma), and 0.1% saponin. MAb screening concentrations were determined using an independent immunofluorescence titration curve against cells expressing wild-type S protein to ensure that signals were within the linear range of detection. Antibodies were detected using 3.75 µg/mL of AlexaFluor488-conjugated secondary antibody (Jackson ImmunoResearch Laboratories 109–545–003) in 10% normal goat serum with 0.1% saponin. Cells were washed three times with PBS++/0.1% saponin followed by two washes in PBS and mean cellular fluorescence was detected using a high-throughput Intellicyt iQue flow cytometer (Sartorius). Antibody reactivity against each mutant S protein clone was calculated relative to wild-type S protein reactivity by subtracting the signal from mock-transfected controls and normalizing to the signal from wild-type S-transfected controls. Mutations within clones were identified as critical to the mAb epitope if they did not support reactivity of the test mAb but supported reactivity of other SARS-CoV-2 antibodies. This counter-screen strategy facilitates the exclusion of S mutants that are locally misfolded or have an expression defect. Validated critical residues represent amino acids whose side chains make the highest energetic contributions to the mAb-epitope interaction.<sup>59,60</sup>

A subset of antibodies was also submitted for epitope mapping by high-throughput SPR and negative-stain electron microscopy by the CoVIC consortium. IgGs were cleaved by

either IdeS (Promega) or papain (Sigma) and purified by ion-exchange chromatography with MonoQ column (GE). Purified Spike trimer (in normal TBS buffer) was mixed with Fabs (1:2 or 2:1 molar ratio) at RT for 3 hours or overnight. Complexes were then purified with Superdex 6. Samples were stained by 0.75% uranyl formate with standard protocol. Datasets were collected by the Halo Titian electron microscope (Thermo Fisher Scientific).

### ***Pseudovirus neutralization assay (IBT)***

Serial semi-log dilutions of antibodies were prepared and mixed with the VSV pseudotype virus in a 1:1 ratio for 1 h at RT followed by incubation over Vero cells (ATCC® CCL-81™) seeded at 60,000 cells per well at 37°C. The cells were lysed the following day and luciferase activity was measured to assess the potency of each antibody to block viral entry into the Vero cells. All samples were tested in triplicate. Data analysis was conducted using XLFit and Prism software (GraphPad).

### ***Authentic virus neutralization assay (USAMRIID)***

Plaque-reduction neutralization testing (PRNT) were performed as described previously (Brocato 2020).<sup>31</sup> Briefly, an equal volume of complete media (EMEM containing 10% heat-inactivated FBS, 1% Pen/Strep, 0.1% Gentamycin, 0.2% Fungizone, cEMEM) containing SARS-CoV-2 USA-WA-1/2020 was combined with antibodies serially diluted twofold in cEMEM. The virus/antibody mixture was incubated at 37°C in a 5% CO<sub>2</sub> for 1 hour and then added to 6-well plates containing 3-day old, ATCC Vero 76 monolayers. After a 1-hour incubation at 37°C, 5% CO<sub>2</sub> incubator a 3 mL per well of agarose overlay (0.6% SeaKem ME agarose, EBME with HEPES, 10% heat-inactivated FBS, 100X NEAA, 1% Pen/Strep, 0.1% Gentamycin and 0.2% Fungizone) was added. The plates were placed in a 37°C, 5% CO<sub>2</sub> incubator for 2 days and then stained with neutral red. PRNT80 titers are the reciprocal of the highest dilution that results in an 80% reduction in the number of plaques relative to the number of plaques visualized in the cEMEM alone (no antibody) wells.

### ***Authentic virus neutralization assay (IBT)***

IBT managed the testing of live wild-type SARS-CoV-2 (USA-WA1/2020 (NR-52281) strain) PRNT assays. Antibodies were tested in triplicate starting at a concentration of 50 µg/mL. Each mAb was serially diluted and incubated with 100 focus-forming units (FFU) of virus at 37°C for 1 h, and added to Vero E6 cell culture monolayers in 96-well plates for 1 h at 37°C to allow for virus adsorption. Cells were then overlaid with 1% methylcellulose in minimum essential medium (MEM) supplemented with 2% FBS. Plates were fixed 30 h later by removing overlays and fixed with 4% paraformaldehyde (PFA) in PBS for 20 min at room temperature. The plates were then incubated with 1 µg/ml of CR3022 antibody<sup>61</sup> and goat anti-human HRP-conjugated IgG (Sigma-Aldrich A6029) in PBS with 0.1% saponin (Sigma-Aldrich 47036) and 0.1% BSA. Staining was visualized by addition of TrueBlue detection reagent (KPL

5510-0030) and quantitated on an ImmunoSpot 5.0.37 Macro Analyzer (Cellular Technologies). Data were processed in Prism (GraphPad). NT<sub>50</sub> and NT<sub>90</sub> represent the antibody concentration required to reduce the number of plaques by 50% or 90%, respectively, compared to free virus.

### ***Evaluation of pre-exposure efficacy in immunosuppressed Syrian hamster model of COVID-19 disease***

Eight- to ten-week-old female Syrian hamsters were immunosuppressed using cyclophosphamide (140 mg/kg day 3 days before challenge and then 100 mg/kg every 4 days by intraperitoneal (i.p.) route). Groups containing six hamsters each were injected with either antibody or nanobody, positive control (convalescent plasma), or a negative control (human mouse chimeric mAb c7D11<sup>59</sup>) on day -1 relative to challenge administered i.p. in a total volume of 2.5 mL/animal. On Day 0 all hamsters were exposed to a target dose of 1,000 PFU SARS-CoV-2 USA-WA-1/2020 isolate by the intranasal route and weighed daily.

### ***Evaluation of post-exposure efficacy in weight loss Syrian hamster model of COVID-19 disease***

Thirty-two, male and female, Golden Syrian hamsters (6–8 weeks old) were split into 4 study groups of 8 hamsters each and weighed prior to start of study. Each group received two doses of vehicle (PBS) or TB202-3 at 1.5 mg/kg at various time points between day 0 and day 3 (*i.e.*, 6 & 48 H, 12 & 48 H, and 24 & 72 H) after intranasal challenge with SARS-CoV-2 ( $5.0 \times 10^4$  TCID<sub>50</sub>) as described in Tostanoski et al.<sup>31</sup> The hamsters from each group were split into two cohorts (A & B) of 4 animals. Each cohort was monitored (using a weight and health score) for 4 days and terminated on day 4 to examine viral titers in the harvested spleen, heart, liver, brain, nasal tissue, trachea internal mucosa, ileum and kidneys.

### ***Evaluation of the post-exposure efficacy a cocktail anti-SARS-CoV-2 antibody in Syrian hamsters***

A post-exposure hamster model was used to evaluate the efficacy of mAbs administered after SARS-CoV-2 infection. For the mAb cocktail experiment (Figure 6), a cocktail containing 10 mg/kg TB202-63 and 10 mg/kg TB181-36 was used. Fifty-four hamsters were used for this experiment, as outlined in Supplemental Table 3. On Day 0, animals were exposed via intranasal instillation to a target dose of 1,000 pfu of SARS-CoV-2 USA-WA-1/2020 in 50 µL volume. The volume was distributed between both nares. All animals were transiently immunosuppressed via treatment with cyclophosphamide starting on Day -3 (140 mg/kg dose) followed by additional doses (100 mg/kg) on Days 1, 5, and 9.

On the indicated day post-exposure, the nanobody/antibody cocktail or c7D11 was administered i.p. On Day 0, blood samples were collected from Group I for hematology to confirm immunosuppression. Group I was also the control for any adverse effects of cyclophosphamide treatment on the hamsters. Clinical scores and individual animal weights were

recorded daily. Animals in Groups A-I were euthanized on day 14 and lungs were collected for virology and pathology.

## Abbreviations

ACE2: angiotensin-converting enzyme 2; BSA: bovine serum albumin; CDR: complementarity-determining regions; CFU: colony forming unit; CoVIC: Coronavirus Immunotherapeutic Consortium; COVID-19: coronavirus disease 2019; CTD: C-terminal domain; CYP: cyclophosphamide; DMEM: Dulbecco's modified eagle's medium; ELISA: enzyme-linked immunosorbent assay; Fab: antigen-binding fragment; FACS: fluorescence-activating cell sorting; FFU: focus forming units; G3P: gene 3 protein; HRP: horseradish peroxidase; HT-SPR: high-throughput surface plasmon resonance; i.p.: intraperitoneal; IBT: Integrated BioTherapeutics; IgG: immunoglobulin G; mAb: monoclonal antibody; MERS-CoV: Middle East respiratory syndrome-related coronavirus; MFI: mean fluorescence intensity; NS-EM: negative-staining electron microscopy; NT: neutralization titer; NTD: N-terminal domain; PBS: phosphate-buffered saline; PBST: phosphate-buffered saline with tween; PFU: plaque forming units; PRNT: plaque reduction neutralization test; RBD: receptor-binding domain; RCA: rolling circle amplification; S: Spike; SARS-CoV: severe acute respiratory syndrome coronavirus; SARS-CoV-2: severe acute respiratory syndrome coronavirus 2; scFv: single-chain variable fragment; SPR: surface plasmon resonance; TCID<sub>50</sub>: tissue culture infective dose 50; USAMRIID: United States Army Medical Research Institute of Infectious Diseases; VH: heavy-chain variable region; VL: light-chain variable region; VSV: vesicular stomatitis virus.

## Acknowledgment(s)

The authors gratefully acknowledge Pavlo Gilchuk, Seth Zost, Joseph Reidy, Elaine Chen, and Andrew Trivette of Vanderbilt University Medical Center for their help in experiments for isolating mAb genes and designing the TB181 COVID-19 scFv library, as well as the Twist Bioscience library team for the design and synthesis of all libraries. We thank Jeff Smith for conducting PRNT, Joshua Moore, Jimmy Fiallos, Steven Stephens for assistance with veterinary care, and Dave Dyer for running hematology at USAMRIID. Additionally, we thank Brian Kearney, Kathleen Gibson and the Unified Culture Collection for providing the virus used at USAMRIID. We would also like to thank Tierra Buck, Colin Mann, and Xiaoying Xu for protein production and assistance with structure determination; Patrick Miller-Rhodes for manuscript preparation; and Catherine J. Hutchings for her critical review and constructive comments on this manuscript. A subset of antibodies was submitted for studies as part of the Coronavirus Immunotherapeutic Consortium (CoVIC), co-supported by the GHR Foundation, NIH NIAID (U19 AI142790-02S1), and the COVID-19 Therapeutics Accelerator, a partnership with funding from the Bill & Melinda Gates Foundation, Wellcome and Mastercard, as well as other private philanthropic support (INV-006133 to LJI). We thank FastGrants from Emergent Ventures at the Mercatus Center, George Mason University for support of essential instrumentation. The work at Vanderbilt was supported by Defense Advanced Research Projects Agency (DARPA) grant HR0011-18-2-0001, U.S. N.I.H. contract 75N93019C00074, and the Dolly Parton COVID-19 Research Fund. J.E.C. is a recipient of the 2019 Future Insight Prize from Merck KGaA, which supported this work with a grant. The opinions, interpretations, conclusions, and recommendations contained herein are those of the authors and are not necessarily endorsed by the US Department of Defense.

## Disclosure statement

This research is sponsored by Twist Bioscience, and authors TZY, LW, EK, ALH, ET, ENS, QL, FA, and AKS are employees of Twist Bioscience. JRW and PG are former employees of Twist Bioscience. BJD, MEF, ED are employees of Integral Molecular. SK and MJA are employees of Integrated BioTherapeutics. JEC has served as a consultant for Luna Biologics, is a member of the Scientific Advisory Board of Meissa Vaccines and is

Founder of IDBiologics. The Crowe laboratory at Vanderbilt University Medical Center has received sponsored research agreements from Takeda Vaccines, IDBiologics and AstraZeneca.

## Funding

The author(s) reported there is no funding associated with the work featured in this article.

## ORCID

James E. Crowe  <http://orcid.org/0000-0002-0049-1079>

## Ethics

Animal research was conducted under an IACUC approved protocol at USAMRIID (USDA Registration Number 51-F-00211728 & OLAW Assurance Number A3473-01) in compliance with the Animal Welfare Act and other federal statutes and regulations relating to animals and experiments involving animals. The facility where this research was conducted is fully accredited by the Association for Assessment and Accreditation of Laboratory Animal Care, International and adheres to principles stated in the Guide for the Care and Use of Laboratory Animals, National Research Council, 2011.

## References

1. Zhou P, Yang X-L, Wang X-G, Hu B, Zhang L, Zhang W, Si H-R, Zhu Y, Li B, Huang C-L, et al. A pneumonia outbreak associated with a new coronavirus of probable bat origin. *Nature*. 2020;579(7798):270–17. [Internet]. doi:10.1038/s41586-020-2012-7.
2. Wu F, Zhao S, Yu B, Chen Y-M, Wang W, Song Z-G, Hu Y, Tao Z-W, Tian J-H, Pei -Y-Y, et al. A new coronavirus associated with human respiratory disease in China. *Nature*. 2020;579(7798):265–69. [Internet]. doi:10.1038/s41586-020-2008-3.
3. Zhu N, Zhang D, Wang W, Li X, Yang B, Song J, Zhao X, Huang B, Shi W, Lu R, et al. A novel coronavirus from patients with pneumonia in china, 2019. *N Engl J Med*. 2020;382(8):727–33. [Internet]. doi:10.1056/NEJMoa2001017.
4. Dong E, Du H, Gardner L. A n interactive web-based dashboard to track COVID-19 in real time. *Lancet Infect Dis*. 2020;20(5):533–34. [Internet]. doi:10.1016/S1473-3099(20)30120-1.
5. Piyush R, Rajarshi K, Khan R, Ray S. Convalescent plasma therapy: a promising coronavirus disease 2019 treatment strategy. *Open Biol*. 2020;10(9):200174. [Internet]. doi:10.1098/rsob.200174.
6. Tanne JH. Covid-19: FDA approves use of convalescent plasma to treat critically ill patients. *BMJ*. 2020;368:m1256. [Internet]. doi:10.1136/bmj.m1256.
7. Sullivan HC, Roback JD. Convalescent plasma: therapeutic hope or hopeless strategy in the SARS-CoV-2 pandemic. *Transfus Med Rev*. 2020;34(3):145–50. [Internet]. doi:10.1016/j.tmr.2020.04.001.
8. Focosi D, Anderson AO, Tang JW, Tuccori M. Convalescent plasma therapy for COVID-19: state of the art. *Clin Microbiol Rev*. 2020;33(4). [Internet]. doi:10.1128/CMR.00072-20.
9. Wang QQ, Zhang Y, Wu L, Niu S, Song C, Zhang Z, Lu G, Qiao C, Hu Y, Yuen K-Y-Y, et al. Structural and functional basis of SARS-CoV-2 entry by using human ACE2. *Cell*. 2020;181(4):1–11. [Internet]. doi:10.1016/j.cell.2020.03.045.
10. Hoffmann M, Kleine-Weber H, Schroeder S, Krüger N, Herrler T, Erichsen S, Schiergens TS, Herrler G, Wu N-H-H, Nitsche A, et al. SARS-CoV-2 cell entry depends on ACE2 and TMPRSS2 and is blocked by a clinically proven protease inhibitor. *Cell*. 2020;181(2):271–280.e8. [Internet]. doi:10.1016/j.cell.2020.02.052.
11. Yan R, Zhang Y, Li Y, Xia L, Guo Y, Zhou Q. Structural basis for the recognition of SARS-CoV-2 by full-length human ACE2. *Science* (80-). 2020;367(6485):1444–48. [Internet]. doi:10.1126/science.abb2762.



12. Liu L, Wang P, Nair MS, Yu J, Rapp M, Wang Q, Luo Y, Chan JF-W, Sahi V, Figueroa A, et al. Potent neutralizing antibodies against multiple epitopes on SARS-CoV-2 spike. *Nature*. 2020;584(7821):450–56. [Internet]. doi:10.1038/s41586-020-2571-7.
13. Huo J, Zhao Y, Ren J, Zhou D, Duyvesteyn HME, Ginn HM, Carrique L, Malinauskas T, Ruza RR, Shah PNM, et al. Neutralization of SARS-CoV-2 by destruction of the prefusion spike. *Cell Host Microbe*. 2020;28(3):445–454.e6. [Internet]. doi:10.1016/j.chom.2020.06.010.
14. Rogers TF, Zhao F, Huang D, Beutler N, Burns A, He W, Limbo O, Smith C, Song G, Woehl J, et al. Isolation of potent SARS-CoV-2 neutralizing antibodies and protection from disease in a small animal model. *Science* (80-). 2020;369(6506):956–63. [Internet]. doi:10.1126/science.abc7520.
15. Zost SJ, Gilchuk P, Chen RE, Case JB, Reidy JX, Trivette A, Nargi RS, Sutton RE, Suryadevara N, Chen EC, et al. Rapid isolation and profiling of a diverse panel of human monoclonal antibodies targeting the SARS-CoV-2 spike protein. *Nat Med*. 2020;26(9):1422–27. [Internet]. doi:10.1038/s41591-020-0998-x.
16. Chi X, Yan R, Zhang JJ, Zhang G, Zhang Y, Hao M, Zhang Z, Fan P, Dong Y, Yang Y, et al. A neutralizing human antibody binds to the N-terminal domain of the spike protein of SARS-CoV-2. *Science* (80-). 2020;369(6504):650–55. [Internet]. doi:10.1126/science.abc6952.
17. Brouwer PJM, Caniels TG, van der Straten K, Snitselaar JL, Aldon Y, Bangaru S, Torres JL, Okba NMA, Claireaux M, Kerster G, et al. Potent neutralizing antibodies from COVID-19 patients define multiple targets of vulnerability. *Science* (80-). 2020;369(6504):643–50. [Internet]. doi:10.1126/science.abc5902.
18. McCallum M, De Marco A, Lempp FA, Tortorici MA, Pinto D, Walls AC, Beltramello M, Chen A, Liu Z, Zatta F, et al. N-terminal domain antigenic mapping reveals a site of vulnerability for SARS-CoV-2. *Cell*. 2021;184(9):2332–2347.e16. [Internet]. doi:10.1016/j.cell.2021.03.028.
19. Wu Y, Jiang S, Ying T. Single-domain antibodies as therapeutics against human viral diseases. *Front Immunol*. 2017;8:1802. [Internet]. doi:10.3389/fimmu.2017.01802.
20. Respaud R, Vecellio L, Diot P, Heuzé-Vourc'h N. Nebulization as a delivery method for mAbs in respiratory diseases. *Expert Opin Drug Deliv*. 2015;12(6):1027–39. [Internet]. doi:10.1517/17425247.2015.999039.
21. Esparza TJ, Martin NP, Anderson GP, Goldman ER, Brody DL. High affinity nanobodies block SARS-CoV-2 spike receptor binding domain interaction with human angiotensin converting enzyme. *Sci Rep*. 2020;10(1):22370. [Internet]. doi:10.1038/s41598-020-79036-0.
22. Cortez-Retamozo V, Lauwereys M, Hassanzadeh Gh G, Gobert M, Conrath K, Muyldermans S, De BP, Revets H. Efficient tumor targeting by single-domain antibody fragments of camels. *Int J Cancer*. 2002;98(3):456–62. [Internet]. doi:10.1002/ijc.10212.
23. Ter Meulen J, Van Den Brink EN, Poon LLMM, Marissen WE, Leung CSWW, Cox F, Cheung CY, Bakker AQ, Bogaards JA, van Deventer E, et al. Human monoclonal antibody combination against SARS coronavirus: synergy and coverage of escape mutants. *PLoS Med*. 2006;3(7):e237. [Internet]. doi:10.1371/journal.pmed.0030237.
24. Shim H. Synthetic approach to the generation of antibody diversity. *BMB Rep*. 2015;48(9):489–94. [Internet]. doi:10.5483/BMBRep.2015.48.9.120.
25. Öling D, Lawenius L, Shaw W, Clark S, Kettleborough R, Ellis T, Larsson N, Wigglesworth M. Large scale synthetic site saturation GPCR libraries reveal novel mutations that alter glucose signaling. *ACS Synth Biol*. 2018;7(9):2317–21. [Internet]. doi:10.1021/acssynbio.8b00118.
26. Immuno precise announces data from preclinical study of TATX-03 POLYTope<sup>TM</sup> monoclonal antibody cocktail candidate against COVID-19 [press release]. Accessed 19 February 2021. Retrieved from <https://www.businesswire.com/news/home/20210219005110/en/ImmunoPrecise-Announces-Data-from-Preclinical-Study-of-TATX-03-PolyTope%E2%84%A2-Monoclonal-Antibody-Cocktail-Candidate-Against-COVID-19>.
27. Madeira F, Park YM, Lee J, Buso N, Gur T, Madhusoodanan N, Basutkar P, Tivey ARN, Potter SC, Finn RD, et al. The EMBL-EBI search and sequence analysis tools APIs in 2019. *Nucleic Acids Res*. 2019;47(W1):W636–W641. doi:10.1093/nar/gkz268.
28. Letunic I, Bork P. Interactive tree of life (iTOL) v5: an online tool for phylogenetic tree display and annotation. *Nucleic Acids Res*. 2021;49(W1):W293–6. doi:10.1093/nar/gkab301.
29. Li W, Moore MJ, Vasilieva N, Sui J, Wong SK, Berne MA, Somasundaran M, Sullivan JL, Luzuriaga K, Greenough TC, et al. Angiotensin-converting enzyme 2 is a functional receptor for the SARS coronavirus. *Nature*. 2003;426(6965):450–54. [Internet]. doi:10.1038/nature02145.
30. Yurkovetskiy L, Wang X, Pascal KE, Tomkins-Tinch C, Nyalile TP, Wang Y, Baum A, Diehl WE, Dauphin A, Carbone C, et al. Structural and functional analysis of the D614G SARS-CoV-2 spike protein variant. *Cell*. 2020;183(3):739–751.e8. [Internet]. doi:10.1016/j.cell.2020.09.032.
31. Brocato RL, Principe LM, Kim RK, Zeng X, Williams JA, Liu Y, Li R, Smith JM, Golden JW, Gangemi D, et al. Disruption of adaptive immunity enhances disease in SARS-CoV-2-infected syrian hamsters. *J Virol*. 2020;94(22):1–13. [Internet]. doi:10.1128/JVI.01683-20.
32. Tostanoski LH, Wegmann F, Martinot AJ, Loos C, McMahan K, Mercado NB, Yu J, Chan CN, Bondoc S, Starke CE, et al. Ad26 vaccine protects against SARS-CoV-2 severe clinical disease in hamsters. *Nat Med*. 2020;26(11):1694–700. [Internet]. doi:10.1038/s41591-020-1070-6.
33. Mucker EM, Wollen-Roberts SE, Kimmel A, Shamblin J, Sampey D, Hooper JW, Geisbert T. Intranasal monkeypox marmoset model: prophylactic antibody treatment provides benefit against severe monkeypox virus disease. *PLoS Negl Trop Dis* [Internet]. 2018;12(6):e0006581. doi:10.1371/journal.pntd.0006581.
34. Marovich M, Mascola JR, Cohen MS. monoclonal antibodies for prevention and treatment of COVID-19. *JAMA*. 2020;324(2):131. [Internet]. doi:10.1001/jama.2020.10245.
35. Zost SJ, Gilchuk P, Case JB, Binshtein E, Chen RE, Nkolola JP, Schäfer A, Reidy JX, Trivette A, Nargi RS, et al. Potently neutralizing and protective human antibodies against SARS-CoV-2. *Nature*. 2020;584(7821):443–49. [Internet]. doi:10.1038/s41586-020-2548-6.
36. Lou Y, Zhao W, Wei H, Chu M, Chao R, Yao H, Su J, Li Y, Li X, Cao Y, et al. Cross-neutralization of RBD mutant strains of SARS-CoV-2 by convalescent patient derived antibodies. *Biotechnol J*. 2021;16(11):2100207. [Internet]. doi:10.1002/biot.202100207.
37. Parry HA, Chiranjivi AK, Asthana S, Yadav N, Shrivastava T, Mani S, Sharma C, Vishwakarma P, Das S, Pindari K, et al. Identification of an anti-SARS-CoV-2 receptor-binding domain-directed human monoclonal antibody from a naïve semisynthetic library. *J Biol Chem*. 2020;295(36):12814–21. [Internet]. doi:10.1074/jbc.AC120.014918.
38. Wu Y, Li C, Xia S, Tian X, Kong Y, Wang Z, Gu C, Zhang R, Tu C, Xie Y, et al. Identification of human single-domain antibodies against SARS-CoV-2. *Cell Host Microbe*. 2020;27(6):891–898.e5. [Internet]. doi:10.1016/j.chom.2020.04.023.
39. Hastie KM, Li H, Bedinger D, Schendel SL, Dennison SM, Li K, Rayaprolu V, Yu X, Mann C, Zandonatti M, et al. Defining variant-resistant epitopes targeted by SARS-CoV-2 antibodies: a global consortium study. *Science* (80-). 2021;374(6566):472–78. [Internet]. doi:10.1126/science.abb2315.
40. Ke Z, Oton J, Qu K, Cortese M, Zila V, McKeane L, Nakane T, Zivanov J, Neufeldt CJ, Cerikan B, et al. Structures and distributions of SARS-CoV-2 spike proteins on intact virions. *Nature*. 2020;588(7838):498–502. [Internet]. doi:10.1038/s41586-020-2665-2.



41. Yuan M, Wu NC, Zhu X, Lee -C-C-CD, So RTYY, Lv H, Mok CKPP, Wilson IA. A highly conserved cryptic epitope in the receptor binding domains of SARS-CoV-2 and SARS-CoV. *Science* (80-). 2020;368(6491):630–33. [Internet]. doi:10.1126/science.abd7269.
42. Wrobel AG, Benton DJ, Hussain S, Harvey R, Martin SR, Roustian C, Rosenthal PB, Skehel JJ, Gambelin SJ. Antibody-mediated disruption of the SARS-CoV-2 spike glycoprotein. *Nat Commun*. 2020;11(1):5337. [Internet]. doi:10.1038/s41467-020-19146-5.
43. Piccoli L, Park Y-J, Tortorici MA, Czudnochowski N, Walls AC, Beltramello M, Silacci-Fregni C, Pinto D, Rosen LE, Bowen JE, et al. Mapping neutralizing and immunodominant sites on the SARS-CoV-2 spike receptor-binding domain by structure-guided high-resolution serology. *Cell*. 2020;183(4):1024–1042.e21. [Internet]. doi:10.1016/j.cell.2020.09.037.
44. Lim SA, Gramespacher JA, Pance K, Rettko NJ, Solomon P, Jin J, Lui I, Elledge SK, Liu J, Bracken CJ, et al. Bispecific VH/Fab antibodies targeting neutralizing and non-neutralizing spike epitopes demonstrate enhanced potency against SARS-CoV-2. *MAbs*. 2021;13(1):1893426. [Internet]. doi:10.1080/19420862.2021.1893426.
45. Li D, Edwards RJ, Manne K, Martinez DR, Schäfer A, Alam SM, Wiehe K, Lu X, Parks R, Sutherland LL, et al. The functions of SARS-CoV-2 neutralizing and infection-enhancing antibodies in vitro and in mice and nonhuman primates. *bioRxiv Prepr Serv Biol*. [Internet] 2021; Available from. <http://www.ncbi.nlm.nih.gov/pubmed/33442694><http://www.pubmedcentral.nih.gov/articlerender.fcgi?artid=PMC7805451>
46. Liu H, Wu NC, Yuan M, Bangaru S, Torres JL, Caniels TG, van Schooten J, Zhu X, Lee -C-CD, Brouwer PJM, et al. Cross-neutralization of a SARS-CoV-2 antibody to a functionally conserved site is mediated by avidity. *Immunity*. 2020;53(6):1272–1280.e5. [Internet]. doi:10.1016/j.immuni.2020.10.023.
47. Seydoux E, Homad LJ, MacCamy AJ, Parks KR, Hurlburt NK, Jennewein MF, Akins NR, Stuart AB, Wan YH, Feng J, et al. Characterization of neutralizing antibodies from a SARS-CoV-2 infected individual. *bioRxiv* [Internet]. 2020. doi:10.1101/2020.05.12.091298.
48. Kreer C, Zehner M, Weber T, Ercanoglu MS, Gieselmann L, Rohde C, Halwe S, Korenkov M, Schommers P, Vanshylla K, et al. longitudinal isolation of potent near-germline SARS-CoV-2-neutralizing antibodies from COVID-19 patients. *Cell*. 2020;182(6):1663–73. [Internet]. doi:10.1016/j.cell.2020.08.046.
49. Cerutti G, Guo Y, Zhou T, Gorman J, Lee M, Rapp M, Reddem ER, Yu J, Bahna F, Bimela J, et al. Potent SARS-CoV-2 neutralizing antibodies directed against spike N-terminal domain target a single supersite. *Cell Host Microbe*. 2021;29(5):819–833.e7. [Internet]. doi:10.1016/j.chom.2021.03.005.
50. Sharma HB, Panigrahi S, Sarmah AK, Dubey BK, Suryadevara N, Shrihari S, Gilchuk P, VanBlargan LA, Binshtein E, Zost SJ, et al. Neutralizing and protective human monoclonal antibodies recognizing the N-terminal domain of the SARS-CoV-2 spike protein. *Cell*. 2021;184(9):2316–2331.e15. [Internet]. doi:10.1016/j.cell.2021.03.029.
51. Chen RE, Zhang X, Case JB, Winkler ES, Liu Y, VanBlargan LA, Liu J, Errico JM, Xie X, Suryadevara N, et al. Resistance of SARS-CoV-2 variants to neutralization by monoclonal and serum-derived polyclonal antibodies. *Nat Med*. 2021;27(4):717–26. [Internet]. doi:10.1038/s41591-021-01294-w.
52. Wang P, Nair MS, Liu L, Iketani S, Luo Y, Guo Y, Wang M, Yu J, Zhang B, Kwong PD, et al. Antibody resistance of SARS-CoV-2 variants B.1.351 and B.1.1.7. *Nature*. 2021;593(7857):130–35. [Internet]. doi:10.1038/s41586-021-03398-2.
53. Bertoglio F, Meier D, Langreder N, Steinke S, Rand U, Simonelli L, Heine Pa, Ballmann R, Schneider K-T, Roth KDR, et al. SARS-CoV-2 neutralizing human recombinant antibodies selected from pre-pandemic healthy donors binding at RBD-ACE2 interface. *Nat Commun*. 2021;12(1):1577. [Internet]. doi:10.1038/s41467-021-21609-2.
54. Chi X, Liu X, Wang C, Zhang X, Li X, Hou J, Ren L, Jin Q, Wang J, Yang W. Humanized single domain antibodies neutralize SARS-CoV-2 by targeting the spike receptor binding domain. *Nat Commun*. 2020;11(1):4528. [Internet]. doi:10.1038/s41467-020-18387-8.
55. Noy-Porat T, Makdasi E, Alcalay R, Mechaly A, Levy Y, Bercovich-Kinori A, Zauberman A, Tamir H, Yahalom-Ronen Y, Israeli M, et al. A panel of human neutralizing mAbs targeting SARS-CoV-2 spike at multiple epitopes. *Nat Commun*. 2020;11(1):4303. [Internet]. doi:10.1038/s41467-020-18159-4.
56. Rouet R, Dudgeon K, Christie M, Langley D, Christ D. Fully human vh single domains that rival the stability and cleft recognition of camelid antibodies. *J Biol Chem*. 2015;290(19):11905–17. [Internet]. doi:10.1074/jbc.M114.614842.
57. Hsieh C-L, Goldsmith JA, Schaub JM, DiVenere AM, Kuo H-C, Javanmardi K, Le KC, Wrapp D, Lee AG, Liu Y, et al. Structure-based design of prefusion-stabilized SARS-CoV-2 spikes. *Science* (80-). 2020;369(6510):1501–05. [Internet]. doi:10.1126/science.abd0826.
58. Davidson E, Doranz BJ. A high-throughput shotgun mutagenesis approach to mapping B-cell antibody epitopes. *Immunology*. 2014;143(1):13–20. [Internet]. doi:10.1111/imm.12323.
59. Lo Conte L, Chothia C, Janin J. The atomic structure of protein-protein recognition sites 1 Edited by A. R. Fersht. *J Mol Biol*. 1999;285(5):2177–98. [Internet]. doi:10.1006/jmbi.1998.2439.
60. Bogan AA, Thorn KS. Anatomy of hot spots in protein interfaces. *J Mol Biol*. 1998;280(1):1–9. [Internet]. doi:10.1006/jmbi.1998.1843.
61. Ter Meulen J, Bakker ABH, Van Den Brink EN, Weverling GJ, Martina BEE, Haagmans BL, Kuiken T, De Kruif J, Preiser W, Spaan W, et al. Human monoclonal antibody as prophylaxis for SARS coronavirus infection in ferrets. *Lancet*. 2004;363(9427):2139–41. doi:10.1016/S0140-6736(04)16506-9.